Mechanism and Machine Theory 176 (2022) 105010

Contents lists available at ScienceDirect

Mechanism and Machine Theory

journal homepage: www.elsevier.com/locate/mechmt

Research paper

Increase of durability in the area of line contact with curved body geometry

Slavomír Hrček [a], Lukáš Smetanka [a], Ján Šteininger [b,*], Branislav Patin [a]

[a] Department of Design and Mechanical Elements, Faculty of Mechanical Engineering, University of Zilina, Zilina 010 26, Slovakia
[b] Institute of Competitiveness and Innovations, University of Zilina, Zilina 010 26, Slovakia

ARTICLE INFO

Keywords:
Contact stress
Rolling contact
Durability
Simulation
Line contact

ABSTRACT

Increasing the durability of machines and equipment is very desirable today. It mainly applies for special and economically expensive applications. This can be achieved by new design of its parts. The aim of this research is to increase the durability of curved bodies with line contact by changing their shape. The durability of a rolling element with a fully crowned profile and a logarithmic profile were calculated using the contact stress at the point of contact obtained analytically on the basis of Hertz's theory and numerically using the finite element analysis. The durability was calculated analytically based on the theories of Lundberg-Palmgren, Ioannides-Harris and Zaretsky and then compared.

1. Introduction

The stresses and deformations that occur when two bodies come into contact with each other on a small area are called contact stresses. The material of the bodies at the point of contact deforms and high contact stresses are caused. The magnitude of the contact stress and the subsurface stress at the point of contact of the two bodies affects their durability. Thus, the higher is the contact stress, the greater is the subsurface stress and the lower is the durability.

According to Hertz, a point contact occurs when the convex profile of a rolling element has a greater curvature than the concave profile of an element with a raceway along which it rolls. In the case of the same curvature of the convex and the concave profile of the two elements, we speak of a line contact. However, these types of contacts occure in the unloaded state of the two elements. When the elements are in the loaded state, the point contact changes to an ellipse or circle-shaped area. When a line contact is loaded, it changes to the area of a rectangle or trapezoid. However, these are theoretical states of the two elements. In places of the discontinuity of the profile of the rolling element shell, it comes to the increase of the contact stresses to the so-called stress peak. Therefore, the end profiles of the rolling elements have to be modified, e.g. to circular curves or logarithmic profiles in order to eliminate these stress peaks.

According to the available literature [2–5], it is possible to determine contact stresses analytically, for example using the Hertz's theory, or numerically using the finite element method (FEM).

The durability of roller bearings is evaluated usually using the ISO 281 standard [6], which is based on the Lundberg-Palmgren theory [7]. The ISO 281 standard specifies methods for calculating the basic rating life, which is the durability assigned to 90% reliability under ideal conditions. In practice, these are rare cases. According to Kaczor and Raczyński [8], it is necessary to take into

* Corresponding author.
E-mail address: jan.steininger@fstroj.uniza.sk (J. Šteininger).

https://doi.org/10.1016/j.mechmachtheory.2022.105010
Received 13 September 2021; Received in revised form 21 June 2022; Accepted 21 June 2022
Available online 12 July 2022

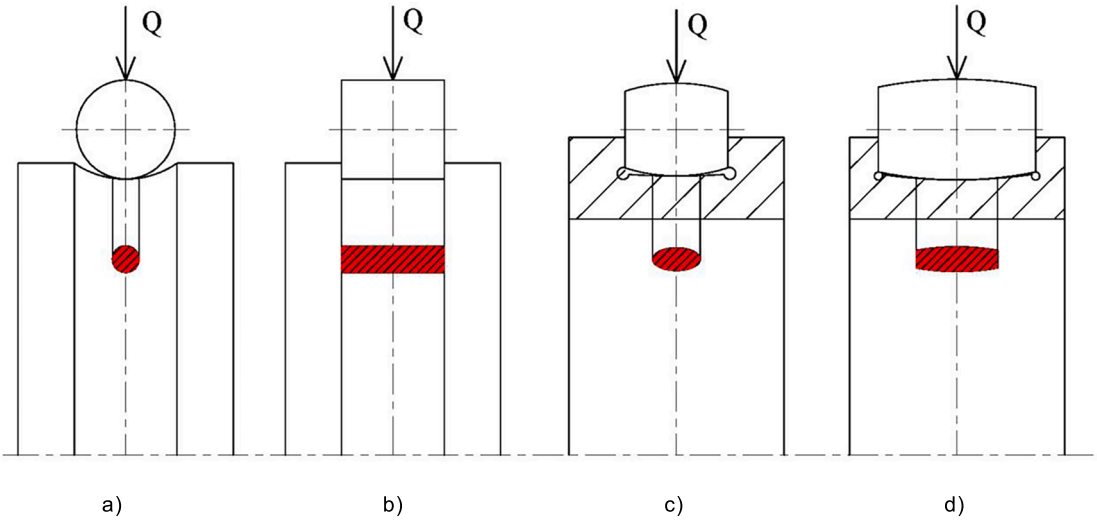

Fig. 1. Types of contact:
(a) point contact; (b) line contact; (c) elliptical contact – open; (d) elliptical contact – closed [1].

account an equivalent dynamic bearing load, i.e., intended equivalent bearing load, corresponding to the assumptions in the calculation of the basic dynamic load rating and having the same effect on the durability as the actual applied acting load. According to Lundberg-Palmgren, the decisive stress for the fatigue of two bodies (the rolling element and the body, e.g., inner or outer ring) is the alternating shear stress inside the material, which changes its direction. Ioannides and Harris theories [9] were based on the Weibull [10] and Lundberg-Palmgren theories, but added the limit fatigue stress and integrated the durability of each elementary volume affected in order to predict the durability of a bearing. Zaretsky [11,12] concludes that the probability of survival depends on the local stress in the affected volume as in Ioannides-Harris, theory but differs from Lundberg-Palmgren theory, which used only one critical stress. According to these theories (Lundberg-Palmgren, Ioannides and Harris and Zaretsky) it is possible to analytically calculate the durability of the two bodies with line contact.

The aim of this paper is to compare the influence of various shape of curved bodies with line contact on the total durability of a bearing utilizing these theories, based on the calculation of the contact stress between these two bodies using the Hertz's theory and FEM [13,14]. Such contact tasks are of great importance in mechanical engineering, since contact stresses arise, for example, between a wheel and a rail in rail vehicles, in roller bearings (wind turbines), or between gears [15–17].

In the case of special applications, the solution brings an increase in the theoretical durability of the bodies (elements). As it will be proven later in the paper, using the logarithmic profile of a curved surface the contact stress can be reduced, unwanted local stress peaks can be removed and thus the related subsurface stress can also be reduced. All these positives will ultimately prove to be advantageous in reducing the weight of the machine components and also in saving considerable material costs during production.

2. Theoretical background

In the case of bodies with curved geometry, three types of contact are distinguished in the contact area. These are the point contact, the line contact and the elliptical contact of bodies [18]. (See Fig. 1)

The shape of the contact area depends on the curvature of the surface of both bodies with surface roughness at the point of contact depending of the production method [19]. The size of the contact area usually increases with increasing load. The formation of the contact area is always associated with the flattening or camber of the bodies at the point of contact and the two bodies approach each other. Plane stress is used for very thin objects. It assumes that stresses in out of plane direction are equal to zero. However, it does not imply that all strain components in that direction are zero too. Plane strain is used for very long objects. It assumes that strains in out of plane direction are equal to zero. But it does not mean that all stress components in that direction must be zero as well. The same empirical formulas apply to the plane stress as well as the plane strain [20], namely

$$E_0 = \frac{E}{1-\frac{1}{\mu^2}}. \tag{1}$$

The nomenclature of all equations used in this study is explained at the end of the article.

We know two-dimensional and three-dimensional line contact. In the case of two-dimensional line contact with a plane strain, the contact area has the shape of a rectangle with the same stress distribution along the entire length of the contact areas. The distribution of the contact stress in the contact area is elliptical. The half-width of the contact area is calculated from the equation

$$b = \left(\frac{8Q}{\pi.E_{I,II}.l_{ef}.\sum q}\right)^{1/2}. \tag{2}$$

Since the curvature of the bodies in the axial direction is zero, for the line contact of the rolling elements applies the equation

$$\sum q = q_{1I} + q_{1II}. \tag{3}$$

In the presented paper, the durability is calculated on the basis of the following described durability theories for roller bearings.

2.1. Lundberg-Palmgren theory

The basic Eq. (5) of the theory includes as a main parameter the stressed amount of material below the surface of the element's raceway. The Eq. (6) determines the orthogonal shear stress in the contact area. This material volume is simplified to a rectangular subsurface cross-sectional area delimited by the length of the ellipse of the maximum contact area and the depth z_o (7), at which the maximum shear stress applied causes a failure to occure. The basic equation is based on the function of the Weibull distribution [10]. The modification of the equation was performed due to the fact that the changes in the state of the material also depend on the depth below the surface of the considered volume element. This assumption must be taken into account by calculating the durability of the roller bearings. Another significant improvement was that Weibull's theory is based on the assumption that the first crack leads to a failure, although this has not been shown to be the case in dealing with fatigue in metals. This is because most cracks never reach the surface of a sample or cause damage. This in turn leads to the assumption that the probability of fatigue failure depends on the above-mentioned depth of the maximum critical shear stress in which the stresses are highest and thus the most dangerous [7]:

$$ln\frac{1}{S} \approx A.\frac{N^e.\tau_0^c.V}{z_0^h}, \tag{5}$$

$$\tau_0 \approx 0,256.p_o, \tag{6}$$

$$z_0 \approx 0,25.2b, \tag{7}$$

$$L_{10} = A\left(\frac{1}{V}\right)^{\left(\frac{1}{e}\right)}\left(\frac{1}{\tau}\right)^{\left(\frac{c}{e}\right)}(z_0)^{\left(\frac{h}{e}\right)} \approx \frac{1}{S_{max}^n}. \tag{8}$$

2.2. Ioannides-Harris theory

Ioannides and Harris theory is based on the Weibull and Lundberg-Palmgren theories, but added the limit fatigue stress τ_u and integrated the durability of each elementary affected volume in order to predict the durability of the bearing. As it can be seen below, the modified form of the Eq. (10) is identical to the Eq. (8) except for the added limit fatigue stress. If the limit fatigue stress τ_u is zero, the Eqs. (8) and (10) are identical:

$$ln\frac{1}{S} \approx A\,N^e\int_V \frac{(\tau-\tau_u)^c}{z^h}dV, \tag{9}$$

$$L_{10} = A\left(\frac{1}{V}\right)^{\left(\frac{1}{e}\right)}\left(\frac{1}{\tau-\tau_u}\right)^{\left(\frac{c}{e}\right)}(z_0)^{\left(\frac{h}{e}\right)} \approx \frac{1}{S_{max}^n}. \tag{10}$$

The main benefit of their combination is the theory that the bearings have a limit fatigue stress. That means, a critical stress less than the fatigue stress would give the bearing an infinite durability. The Ioannides-Harris equation was found to precisely predict the durability of bearings when comparing the calculated results with large-scale tests [9].

2.3. Zaretsky theory

Both Weibull and Lundberg and Palmgren theories combine the exponent of the critical shear stress c with the Weibull slope e. Therefore, the ratio c/e becomes a separate expression in itself, which is commonly referred as the effective exponent of the critical shear stress. This suggests that the variance in the durability of a bearing depends on this critical exponent. Zaretsky found that for a wide range of conditions, most values of a given exponent range from 6 to 12. Based on Zaretsky's findings, he rewrote the Weibull's equation, with the exponent c becoming independent of the Weibull slope e according the equation

$$N \sim \left[\frac{1}{\tau}\right]^c\left[\frac{1}{V}\right]^{1/e}. \tag{11}$$

The resulting equation for durability then has the form

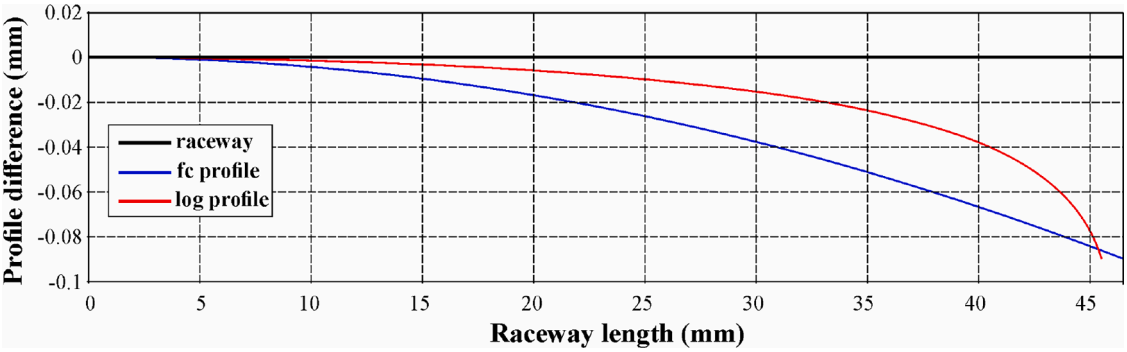

Fig. 2. Fully crowned profile (blue curve) and logarithmic profile (red curve) in the curvature of the rolling element depending on the half-raceway length (For interpretation of the references to color in this figure, the reader is referred to the web version of this article.).

$$L_{10} = A\left(\frac{1}{V}\right)^{\left(\frac{1}{e}\right)}\left(\frac{1}{\tau}\right)^{c}(z_0)^{\left(\frac{h}{e}\right)} \approx \frac{1}{S_{max}^{n}}, \tag{12}$$

where $c = 9$, $e = 1.11$, $n = 9.9$ for the line contact and $n = 10.8$ for the point contact. Conceptually, Zaretsky concludes that the probability of survival depends on the local stress in the affected volume as in Ioannides-Harris theory, but differs from Lundberg-Palmgren theory, which used only one critical stress. Zaretsky also did not include the limit fatigue stress in the equation, but stated in many documents that he did not exclude it [11,12].

2.4. Theory based on ISO 281: 2007

This standard was first published in 1990. Since its publication further knowledge has been gained regarding the effect of contamination of the lubricant on the lubrication, internal stresses from assembly, stresses from hardening, limit fatigue stress of the material on the durability of a bearing and the like, up to the form ISO 281: 2007. The standard specifies methods for calculating the basic dynamic load rating of roller bearings in the range of dimensions corresponding to international ISO standards, with a specified production process. The calculation of durability according to ISO 281 is based on the Lundberg-Palmgren theory. According to the standard, the basic equation of the durability calculation is defined as

$$L_{10} = \left(\frac{C_r}{P_e}\right)^{p}, \tag{13}$$

where L_{10} is the basic rating life, C_r is the basic dynamic load rating, P_e represents the equivalent dynamic bearing load and p is the exponent ($p = 3$ for ball bearings, $p = 10/3$ for spherical roller bearing and tapered roller bearings).

The standard specifies methods for calculating the basic rating life which is the durability assigned to 90% reliability using high quality materials, produced in good conditions and under normal operating conditions. In addition, it stipulates methods for calculating modified durability at various degrees of reliability, lubrication conditions, impurities in the lubricant and limit fatigue loads. Dynamic load rating is the basic and only parameter that describes a specific value of a roller bearing. This is a constant radial load at which the bearing can theoretically reach the basic probable durability at 10^6 revolutions. The formula for its calculation is defined for the roller bearings as

$$C_r = b_m.f_c.\left(i.l_{ef}\cos\alpha\right)^{7/9}.Z^{3/4}.D_{we}^{29/27}, \tag{14}$$

where b_m is the coefficient of basic dynamic load rating, l_{ef} is the effective length of the rolling elements, f_c is the coefficient depending on the bearing geometry and accuracy of production and material, i is the number of rows of rolling elements in the bearing, α is the nominal contact angle [°], Z is the number of rolling elements in a single-row bearing and D_{we} is the nominal rolling element diameter [6].

3. CAD model / FEM simulation

One of the main prerequisites for determination of the durability is the knowledge of the contact stress between bodies (elements) in contact in the investigated system. The required contact stress as well as the subsurface stress are calculated in two ways. The first method was an analytical calculation using the Hertz's theory of contact stress. The Hertz's theory is generally known and we will not deal with its description in the paper. The second way to obtain the contact stress was the numerical calculation using the finite element method (FEM) implemented in the Ansys Workbench software [21,22].

For the needs of the FEM simulation, but also in order to demonstrate the change in durability using geometry with logarithmic

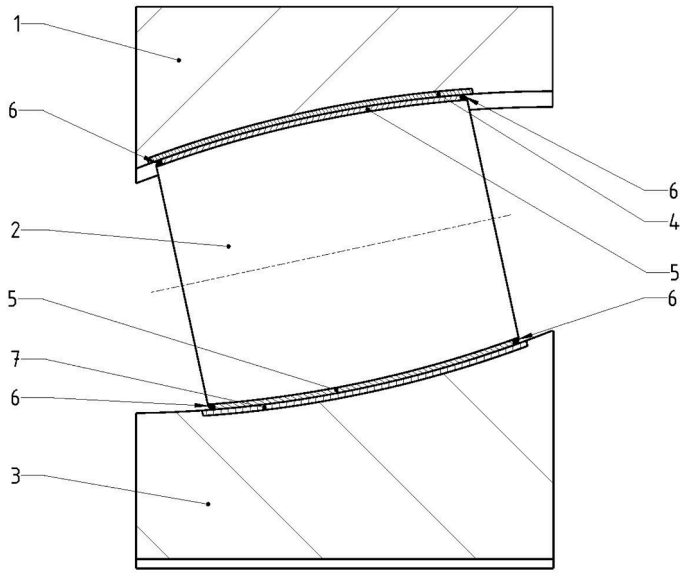

Fig. 3. Cross-section and individual parts of the 3D parametric model of the reference spherical roller bearing: 1 – outer ring; 2 – rolling element; 3 – inner ring; 4 – contact volume on the outer ring; 5 – contact volume on the rolling element; 6 – volume of the rolling element end profile radius; 7 – contact volume on the inner ring.

profile of the contact area, it was necessary to create a 3D virtual model of contact elements with geometry with fully crowned profile (hereinafter referred as *fc* profile) and logarithmic profile (hereinafter referred as *log* profile). The PTC / Creo Parametric software was used to create this parametric 3D virtual model. A spherical roller bearing was used as a reference model, which geometrical parameters are known and available in the bearing catalogues, or from the manufacturer himself. The basis of the model comprises suitably created drawings to which the individual volumes of the bearing elements are subsequently linked [22,23]. In this way, it is possible to operatively change selected bearing parameters with the help of several drawings, and to quickly and easily cover selected dimensional series of spherical roller bearings. The geometry was defined to reflect the actual dimensions of the spherical roller bearing, including all structural elements such as the concave cylinder, the exact radius of the profile curves, etc. This was necessary in order to ensure a correct analysis of the contact stresses as well as to evaluate the subsurface stress.

The distribution and magnitude of the contact stress depends on the geometric shape of the bodies in contact. The aim is to optimize the shape of the individual bodies (elements) to ensure the optimal contact stress and distribution of the subsurface stress [24]. Fig. 2 presents the investigated profile difference of the used geometries without the transition of the profile curves to the end radius.

The size of the end radius of the rolling element is typically dependent on the diameter and length of the rolling element. The rolling element model with the log profile has the same size of the end radius as the model with the standard fc profile, which will ensure that the size of the end radius will not affect the achieved results and they can be then compared objectively.

The *log* profile geometry was created in the contact area of the rolling element. The geometry of the rolling element consists of a logarithmic curve and not circular curves as in the case of the *fc* profile geometry. Dimensions of the bodies with raceways (bearing rings) have been preserved. The logarithmic curve is defined by the equations

$$y = R_e - R_e.\left(1 - \sqrt{1 - \left(\frac{x}{R_e}\right)^2}\right) - d_{log}.\, D_{we}.\ln\left(\frac{1}{\left(1 - \left(2.\frac{x}{l_T}\right)^2\right)}\right), \tag{15}$$

$$x \in \left\langle -\frac{l_T}{2}; +\frac{l_T}{2}\right\rangle \tag{16}$$

The Eq. (15) has a high gradient of decline at the end of the log profile at $x = \pm l_T/2$. Such a body profile would be very difficult to manufacture by standard grinding manufacturing processes, therefore the rolling body profile ends with an end radius, which is tangentially connected to the log profile described by the Eq. (15) in order to reduce the contact pressure peaks.

Due to the most accurate calculation in the FEM analyses, it was necessary to divide the volumes of the contact bodies precisely at the point of contact. The size of these contact volumes for the inner and outer element contact was calculated based on Eqs. (17), (18) for the rolling element – inner ring contact and (19), (20) for the rolling element – outer ring contact. The calculated parameters were used with a correction of + 20%.

The contact volume width b and the depth z_0 (in which τ_0 is applied) of the contact volume for the contact rolling element-inner ring are defined by the equations

Table 1
Element types and sizes of the FEM model sections presented in Fig. 3.

Section of the FEM model in Fig. 3		Element type	Element size (mm)
1	outer ring	SOLID185	5.00
2	rolling element	SOLID185	5.00
3	inner ring	SOLID185	5.00
4	contact volume on the outer ring	SOLID185 / CONTA174	0.25 on the contact surface width 0.50 on the contact surface legth
5	contact volume on the rolling element	SOLID185 / TARGE170	0.25 on the contact surface width 0.50 on the contact surface legth
6	volume of the rolling element end profile radius	SOLID185 / TARGE170	0.40
7	contact volume on the inner ring	SOLID185 / CONTA174	0.25 on the contact surface width 0.50 on the contact surface legth

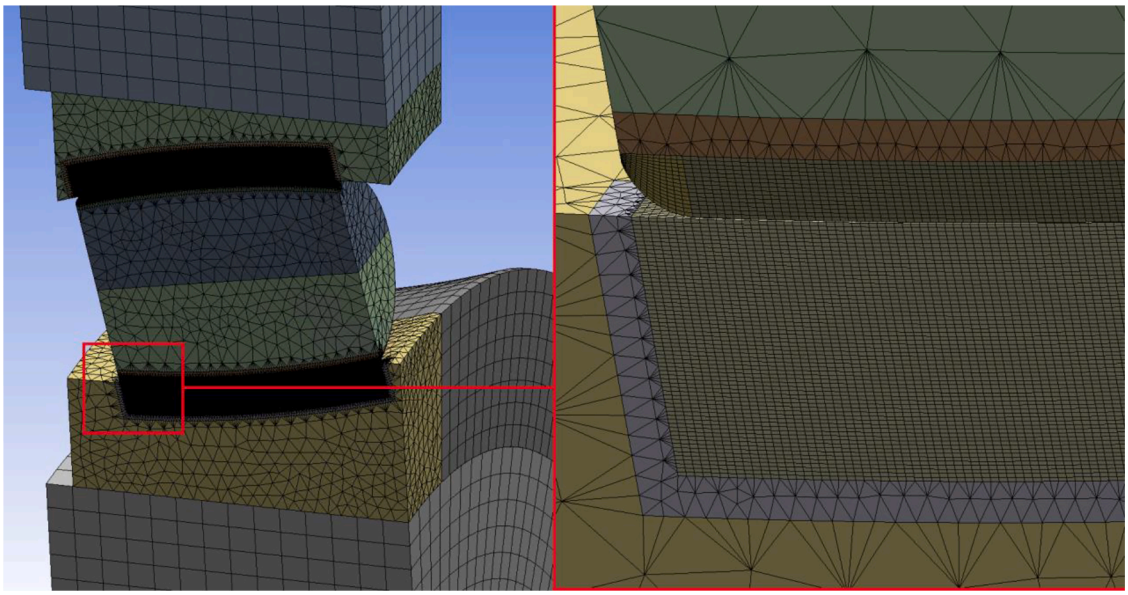

Fig. 4. Finite element network of the investigated bearing:
left- general view; right-detail of the finite element network.

$$b = 2,36.10^{-3}.\sqrt{\frac{Q_{max}}{l_T}.\frac{1}{\frac{1}{D_{we}}+\frac{1}{D_F}}}, \tag{17}$$

$$z_0 \sim 0,5b. \tag{18}$$

The contact volume width b and the depth z_0 (in which τ_0 is applied) of the contact volume for the contact rolling element-outer ring are defined by the equations

$$b = 2,36.10^{-3}.\sqrt{\frac{Q_{max}}{l_T}.\frac{1}{\frac{1}{D_{we}}-\frac{1}{D_E}}}, \tag{19}$$

$$z_0 \sim 0,5b. \tag{20}$$

The static analysis of contact elements was performed using the Ansys Workbench software which allowed the import of the geometry from the PTC / Creo Parametric software. The connection between the PTC / Creo Parametric software and the Ansys Workbench software is advantageous as it allows the geometry and position of the model to be changed by modifying the relevant analysis parameters [25]. The Workbench environment preserves the analysis settings (the definition of boundary conditions, loading forces, etc.) and postprocessing (the evaluation of the analysis results). It is therefore possible to easily and quickly modify the parameters of the investigated elements. An equally important step in the correct analysis of the magnitude of contact and subsurface stresses is the definition of a finite element meshing network [26]. The meshing network of the FEM model for contact stress analysis should be defined by at least five nodes per half the width of the contact area $b/2$. Mesh density along contact profiles has been defined as 3 times the element size along the width of contact area in order to decrease the finite element model computational requirements

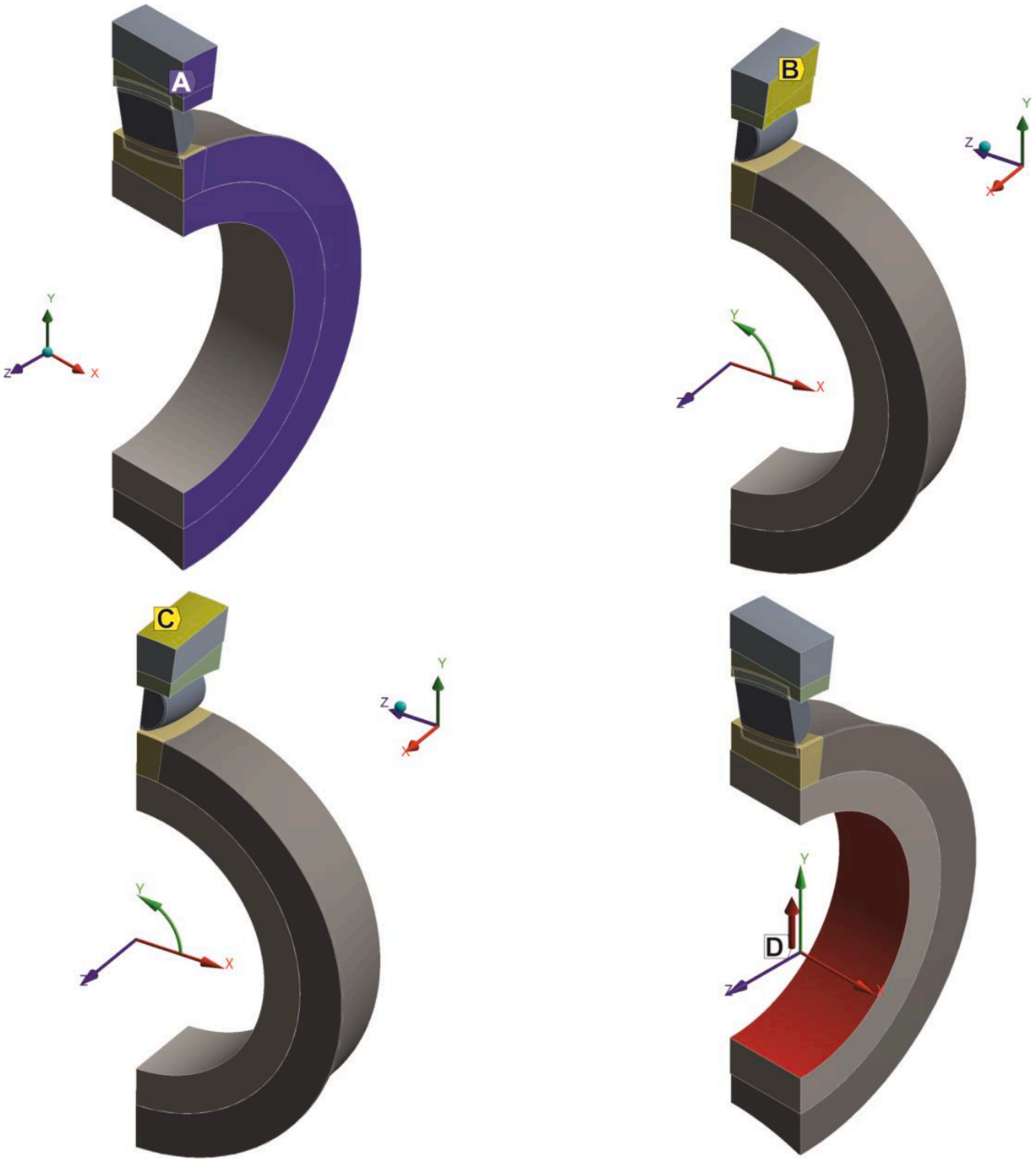

Fig. 5. Calculation boundary conditions.

[27,28]. Mesh of imported 3D geometries was performed in the Ansys Workbench software environment using a Solid 185 element. The individual bearing elements are in contact with each other because the forces acting on the bearing are transmitted among the rings (their raceways) and the individual rolling elements as shown in Fig. 3. Elements of the CONTA 174 and TARGE 170 type were used to define the contact areas of the bearing. Hexagonal volume elements were used in the contact area; in other parts of the bearing were used the tetragonal volume elements. The list of the element types and sizes is presented in Table 1.

The finite element network is shown in Fig. 4.

The spherical roller bearing model was defined for the calculation in half the symmetry of one rolling element. The areas between the objects, which represent the contact volumes between the rolling element and the outer or the inner ring, were defined as

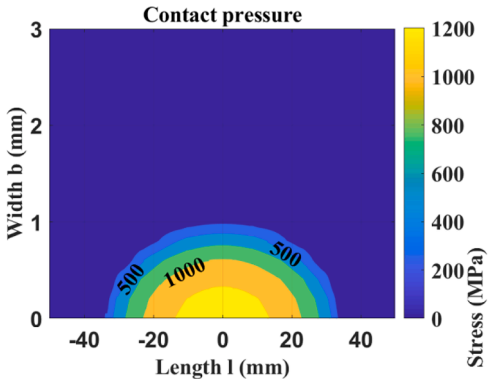

Fig. 6. Distribution of contact stress along the line contact of the fc profile at low load.

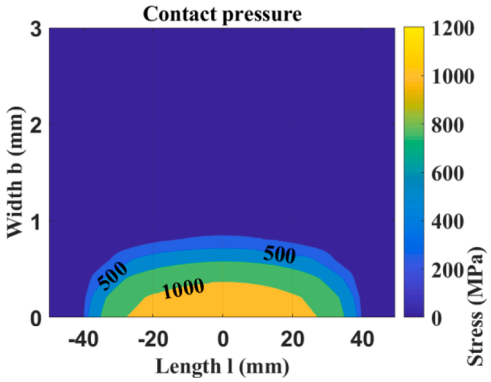

Fig. 7. Distribution of contact stress along the line contact of the log profile at low load.

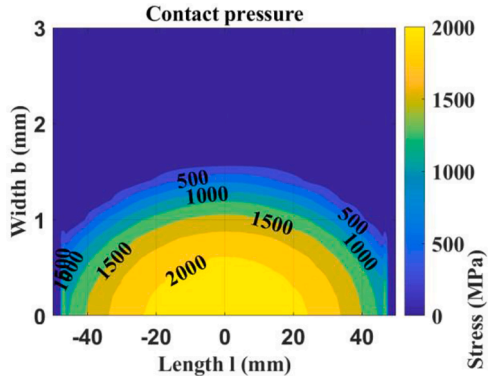

Fig. 8. Distribution of contact stress along the line contact for the fc profile at medium loads.

Frictionless. Boundary conditions (see Fig. 5) were defined for the computational model as follows:

- A – symmetry in the ZY plane.
- B – rotational symmetry in the XY plane.
- C – removal of one degree of freedom in the direction of the *"x"* axis in the cylindrical coordinate system on the surface of the outer ring (retention of the radial force) – prevention of expansion of the outer bearing ring in the radial direction – replacement of the cage / housing.
- D – application of the loading force – the loading of the model was simulated by applying the radial force in the direction of the *"y"* axis to the area of the inner ring and its magnitude is divided into several loading steps.

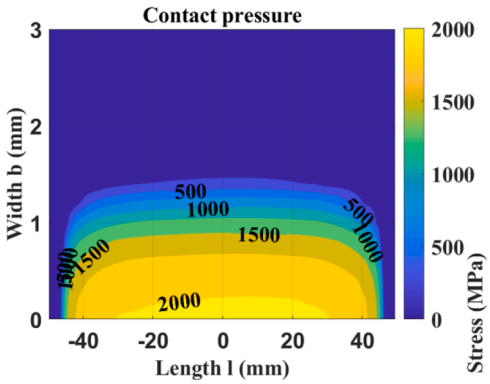

Fig. 9. Distribution of contact stress along the line contact for the log profile at medium loads.

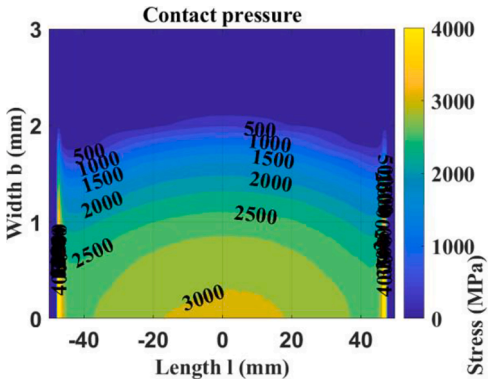

Fig. 10. Distribution of contact stress along the line contact for the fc profile at high loads.

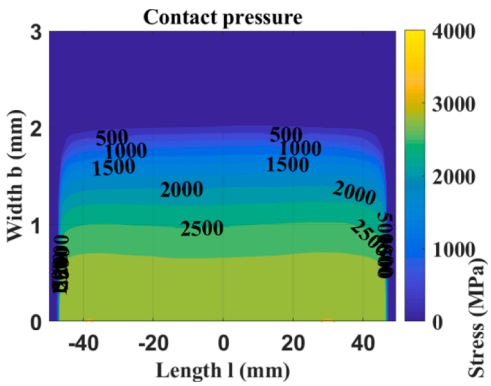

Fig. 11. Distribution of contact stress along the line contact for the log profile at high loads.

The calculation of the contact and subsurface stresses based on the FEM analyses is shown in Figs. 6–11. The graphs show the distribution of the contact stress along the line contact for the *fc* profile and for the *log* profile. A symmetrical model is shown – the half the width of the contact area; the contact stress is shown in a top view of the area. The maximum load rating is determined as the maximum load rating for the elements with line contact, which is approximately at a contact stress of 3500 MPa. The contact stress is calculated for three different portions of maximum load:

- low load (approx. 20% of the max. load) – central area contact stress approx. 1200 MPa.
- medium load (50% of the max. load) – central area contact stress approx. 2000 MPa.
- high load (80 – 100% of the max. load) – central area contact stress approx. 3000 MPa.

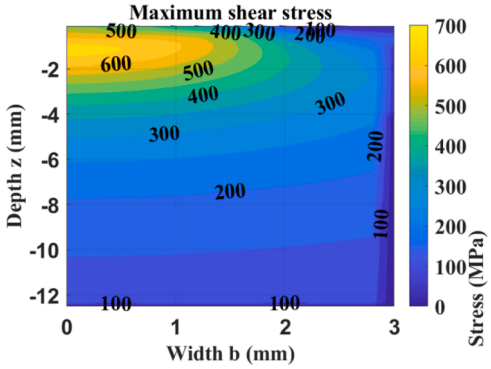

Fig. 12. Distribution of the maximum subsurface shearstress for the fc profile.

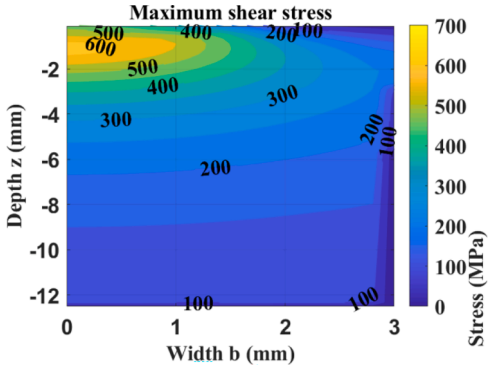

Fig. 13. Distribution of the maximum subsurface shear stress for the log profile.

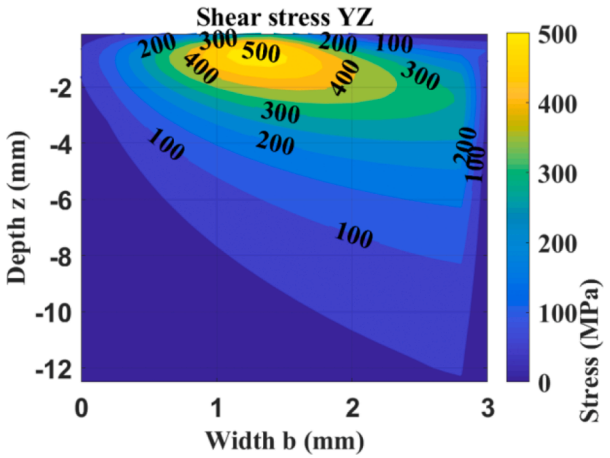

Fig. 14. Distribution of the YZ subsurface shear stress for the fc profile.

The display of the subsurface stresses (Figs. 12–17) is performed for the variants of the *fc* profile and the *log* profile located in the middle cross section of the rolling element and raceway profile.

In all cases, a medium load was applied (central area contact pressure approx. 2000 MPa).

The graphs in Figs. 18–23 show the change in the stress distribution in the contact and subsurface areas between the rolling element with the *fc* profile – the circular curves (blue curve) or the log profile (red curve). The small peak of the *fc* profile contact pressure located in Fig. 18 may be caused by a finite-element mesh error, but such a small value will not affect the results presented in this paper. The subsurface stress analysis is obtained from a point in the middle of the line contact ("YZ" plane). The presented graphs clearly show the fact that in proportion to the decrease ofn the magnitude of the contact stress, the magnitudes of the contact stresses of

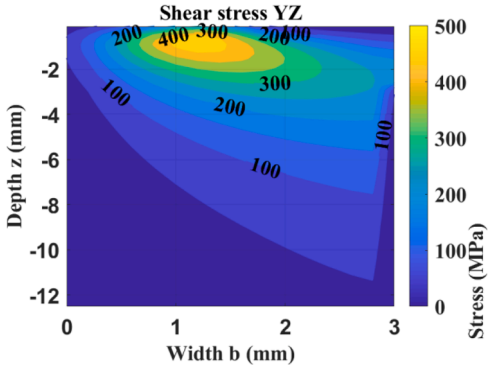

Fig. 15. Distribution of the YZ subsurface shear stress for the log profile.

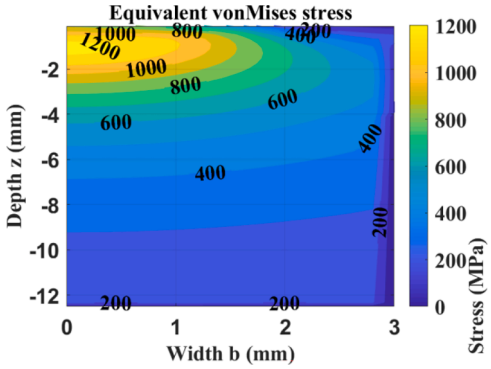

Fig. 16. Distribution of the equivalent von Mises subsurface stress for the fc profile.

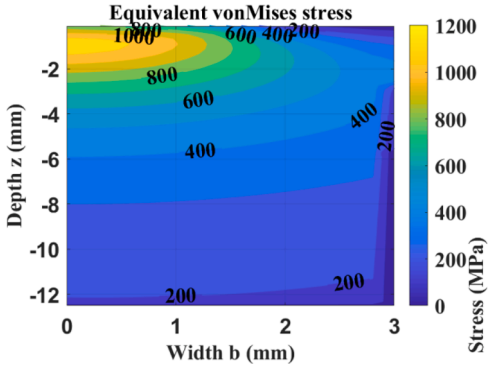

Fig. 17. Distribution of the equivalent von Mises subsurface stress for the log profile.

the line contact also decrease. A significant benefit of the proposed geometry with the *log* profile is the knowledge that the use of this profile already at medium and also at high loads successfully eliminates stress peaks at the end profiles of the contact areas. This phenomenon can only be noticed in Figs. 20 and 22. The subsurface stress is evaluated for the individual stresses as follows:

- σ_x, σ_y, σ_z – principal stresses (dotted lines).
- τ_{max} – maximum shear stress.
- τ_{yz} – shear stress acting in the "YZ" plane.
- σ_{vonM} – equivalent von Mises stress.

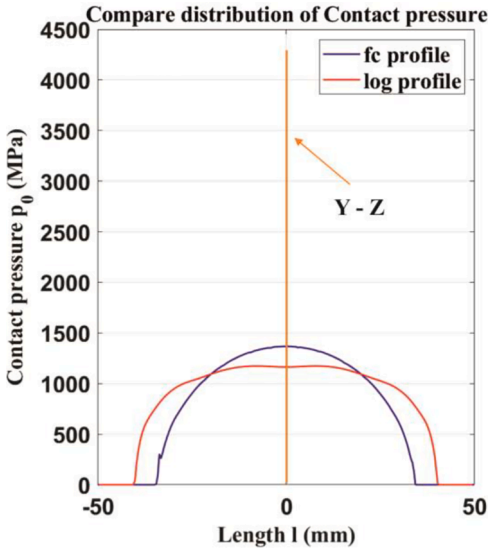

Fig. 18. Distribution of the contact stress along the line contact at low load (For interpretation of the references to color in this figure legend, the reader is referred to the web version of this article.).

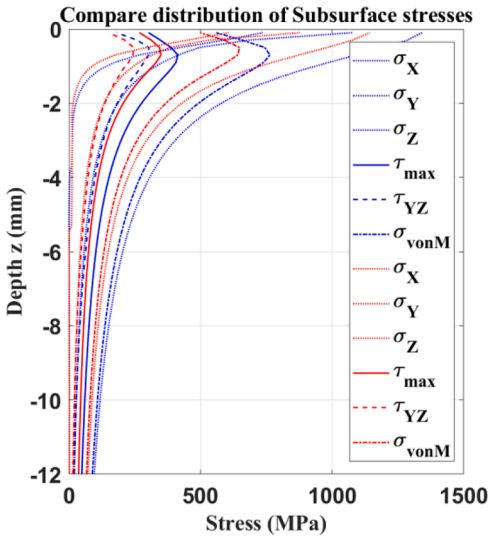

Fig. 19. Subsurface stress at low load (For interpretation of the references to color in this figure legend, the reader is referred to the web version of this article.).

4. Results

For the needs of the calculation of durability according to the ISO standard and especially according to individual theories (of Lundberg-Palmgren, Ioannides-Harris, Zaretsky) a script was created in MATLAB programming language, with the help of which durability was calculated on the basis of the calculated stress obtained from the FEM analysis. The necessity to create a script was mainly due to the need for numerical integration within the theories of Ioannides-Harris and Zaretsky.

The following graphs show a comparison of individual calculation methods (by Lundberg-Palmgren, Ioannides-Harris, Zaretsky) for the geometry formed by the *fc* profile according to ISO/TS 16281 – circular curves and subsequently for the modified geometry formed by the log profile. The calculated durability ("*x*" axis) is displayed depending on the magnitude of the load ("*y*" axis).

Fig. 24 shows the calculated durability for the ideal *B-shape* fully crowned model without stress peaks (*fc* parameter = 0.97), at which the contact stress as well as the subsurface stress are calculated on the basis of the Hertz's contact stress theory (for the analytical calculation see Chapter 3) and compares it with the calculated durability for the FEM model with the *fc* profile (*fc parameter* = 0.97) shown in Fig. 25 and for the FEM model with the *log* profile of the rolling element (*log parameter* = 0.00035) shown in Fig. 26.

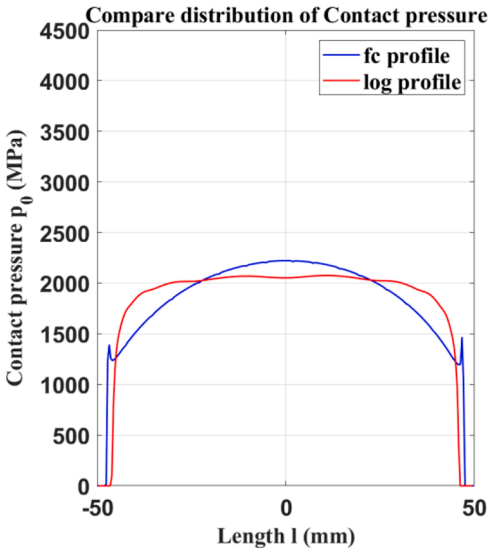

Fig. 20. Distribution of the contact stress along the line contact at medium load (For interpretation of the references to color in this figure legend, the reader is referred to the web version of this article.).

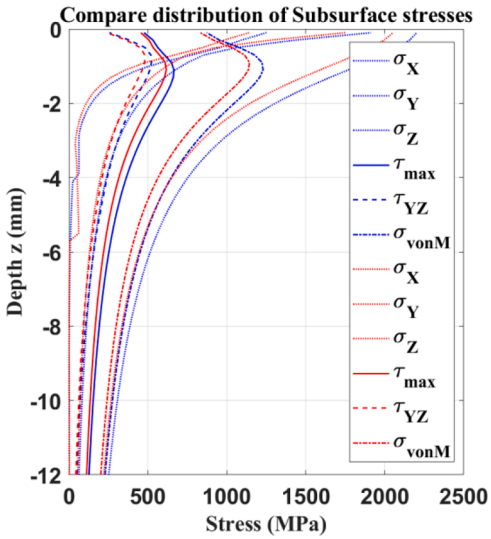

Fig. 21. Subsurface stress at medium load (For interpretation of the references to color in this figure legend, the reader is referred to the web version of this article.).

Unlike Hertz's theory, the FEM models also include stress peaks. Therefore, there is a significant difference in durability when we compare the individual graphs where the ideal line contact shows greater durability for higher load magnitudes. The calculation incorporating stress peaks is considered to be more accurate based on the research.

The following graphs compare the calculated durability for the individual models used by the appropriate theory: Fig. 27 for the Lundberg-Palmgren theory, Fig. 28 for the Ioannides-Harris theory and Fig. 29 for Zaretsky theory. There were used following rolling element models: the *B-shape* theoretical model of an ideal contact of fully crowned solids without stress peaks, the FEM model with the exact description of contact body geometry for the *fc* profile and the FEM model for the *log* profile of the rolling element. For the overall comparison, the durability was also calculated according to the ISO 281 standard.

The Figs. 27–29 show significantly increase of the durability by the use of the shape of the rolling element with the *log* profile in comparison with the geometry formed by the *fc* profile under identical load for each theory used by the durability calculation. This phenomenon is considered to be a big positive, especially in terms of lower stress on the bodies (elements) at the points of contact and thus increase of the machine parts durability.

Following figures show the effect of the change in the ratio between the circular curves of the raceways of the bearing rings and the shell of the rolling element (denoted as the *fc parameter / log parameter*) and the magnitude of the radial load (F_{rad}) on the calculated

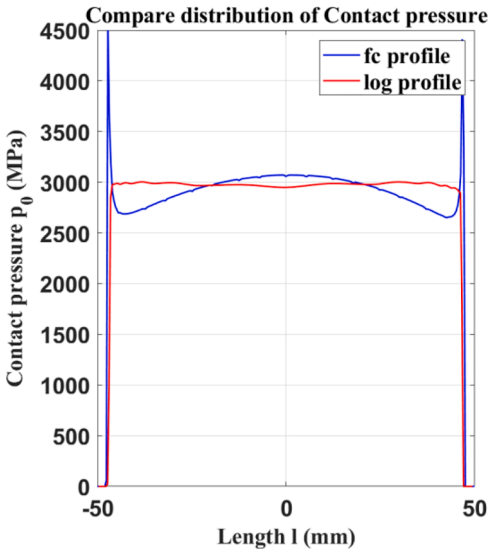

Fig. 22. Distribution of the contact stress along the line contact at high load (For interpretation of the references to color in this figure legend, the reader is referred to the web version of this article.).

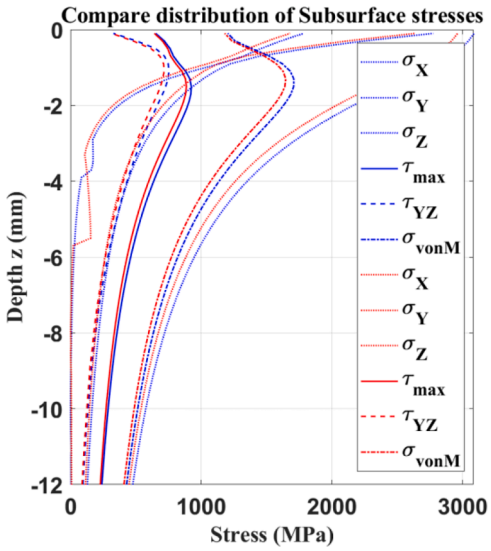

Fig. 23. Subsurface stress at high load (For interpretation of the references to color in this figure legend, the reader is referred to the web version of this article.).

total durability. The analysis was performed according to computational theories (Lundberg-Palmgren, Ioannides-Harris, Zaretsky) for the shape of the rolling element with the *fc* profile (Figs. 30, 32, and 34) and the shape of the rolling element using the log profile (Figs. 31, 33, and 35). The displayed results are conveniently recalculated relative to their maximum for 100% for each variant of the *fc / log parameter*, so the calculated durability for each value reached the maximum of 100%. For all variants, only the calculation based on the data obtained from the finite element analysis (FEM) was used because this calculation results are closest to the real state. The graphs show that the 3D areas are more flat in the shape of the rolling element formed by the log profile than the steeper areas in the geometry formed by the *fc* profile, which means that the *log* profile is more suitable for a wider load range.

In order to better display the steepness of the profiles depending on the magnitude of the load, the curves in graphs below were created. They represent the cross-sections of the 3D areas shown above. These cross-sections were made for different load magnitudes under the same conditions for the *fc* profile (Figs. 36, 38, and 40) and for the geometry of the rolling element formed by the *log* profile (Figs. 37, 39, and 41).

The results of the durability calculation of the rolling element with the *log* profile according to all theories used to calculate the durability, the steepness of the curves is significantly lower compared to the curves for the *fc* profile. It means that for the same load

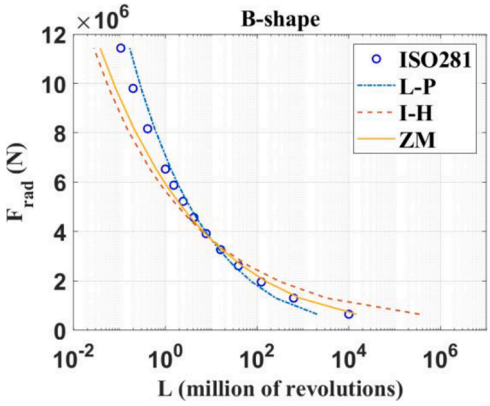

Fig. 24. Durability for the analytical model (*fc* profile).

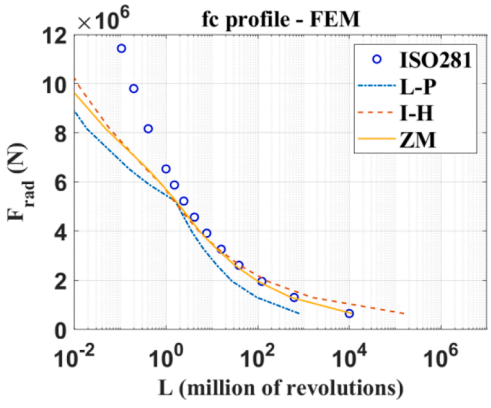

Fig. 25. Durability for the numerical model (*fc* profile).

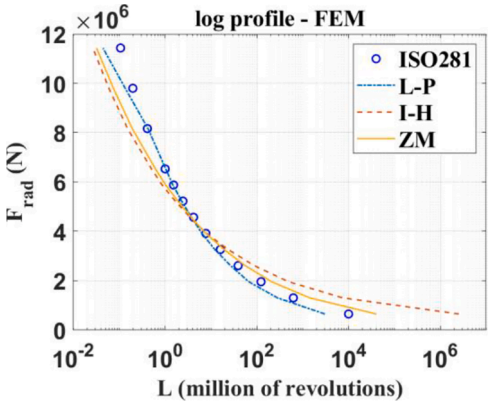

Fig. 26. Durability for the numerical model (*log* profile).

range, the *log* element shape is more advantageous in terms of durability.

The graphs in Figs. 42–44 present the effect of the curve ratio size (*fc parameter*) on durability at different load magnitudes. It is generally known that each contact of two bodies is able to carry only a certain possible load – in the case of bodies (elements) with the line contact, this load can be determined considering the maximum contact stress, which is approximately 3500 MPa. This magnitude represents 100% of the radial force F_{rad} in the graphs shown below. If we want the given line contact to carry low loads (approx. 20% of the max. load), it is appropriate to consider the *fc* parameter at the value of 0.99. If we want to transfer medium loads (approx. 50% of the max. load) by the line contact, it is advisable to consider the *fc* parameter at the value of 0.97. For the last case of transferring very high loads at the limit of the load rating of the line contact itself (approx. 80 – 100% of the maximum), it is appropriate to consider the

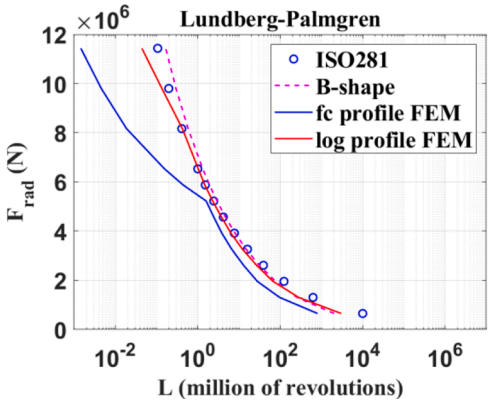

Fig. 27. Calculation of durability according to Lundberg-Palmgren theory (*fc* profile).

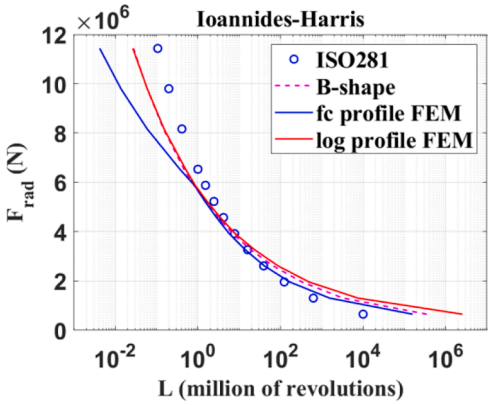

Fig. 28. Calculation of durability according to Ioannides-Harris theory (*fc* profile).

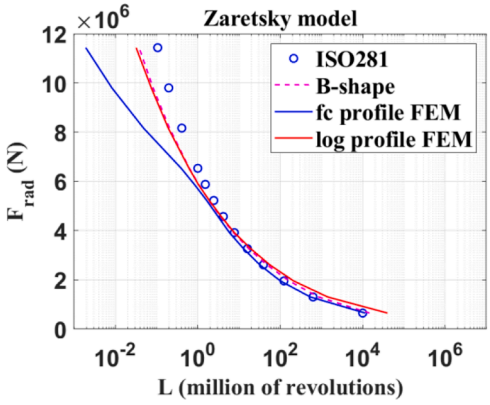

Fig. 29. Calculation of durability according to Zaretsky theory (*fc* profile).

fc parameter at the value of 0.95. This knowledge is very important, if the load system of the particular machine part is known. It is then possible to use the described knowledge by dimensioning and calculation. For example, in the case of roller bearings, the operation will be defined at the beginning of the selection of a suitable bearing. There will be defined how much load will be applied to the bearing during its expected durability and the internal geometry of the roller bearing can be designed appropriate.

The graphs in Figs. 45–47 show the influence of the *log* parameter of the rolling element on the durability at different load magnitudes. If we want the given line contact to transfer small loads (approx. 20% of the max. load), it is ppropriate to consider the *log parameter* at the value of 0.00025. If we want to transfer medium-sized loads (approx. 50% of the max. load) by the line contact, it is advisable to consider a *log parameter* at the value of 0.00035. For the last case of transmitting very high loads at the limit of the load

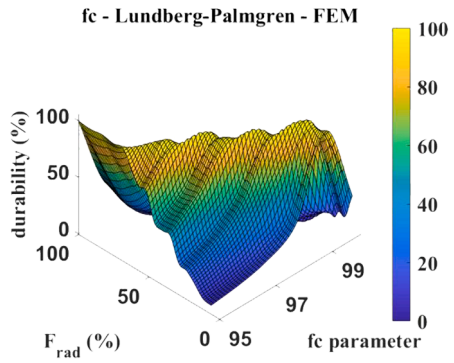

Fig. 30. 3D graph showing the ratio between the *fc* parameter and the magnitude of the load on durability according to Lundberg-Palmgren.

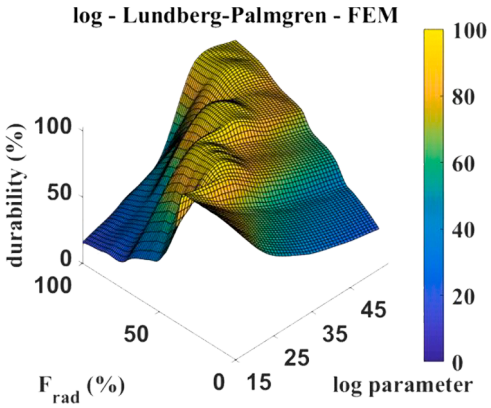

Fig. 31. 3D graph showing the ratio between the log parameter and the magnitude of the load on durability according to Lundberg-Palmgren.

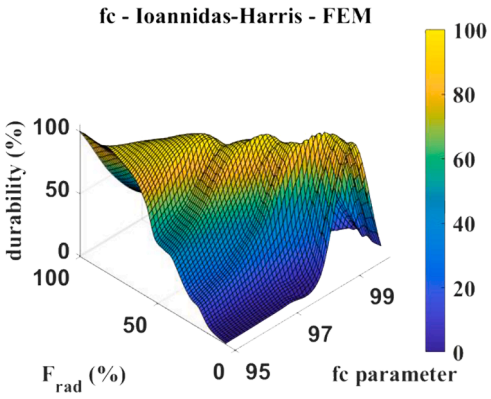

Fig. 32. 3D graph showing the ratio between the *fc* parameter and the magnitude of the load on durability according to Ioannides-Harris.

rating (approx. 80–100% of the max. load) it is suitable to use a *log parameter* at the value of 0.00055.

The shape of the rolling element using the log profile is therefore more suitable for a wider load range than the *fc* profile. The durability graphs according to individual theories for the *fc* profile (Figs. 42–44) are visibly steeper than the durability graphs for the log profile (Figs. 45–47) of the rolling element.

The graphs in Figs. 48–50 compare the durability of the selected values of the *fc* parameter and the *log* parameter. The analysis performed using the above-mentioned theoretical methods as well as the percentage evaluation (Fig. 51) clearly demonstrate a significant positive change in durability in the case of using the geometry of a rolling element with the log profile at a higher radial load F_{rad}.

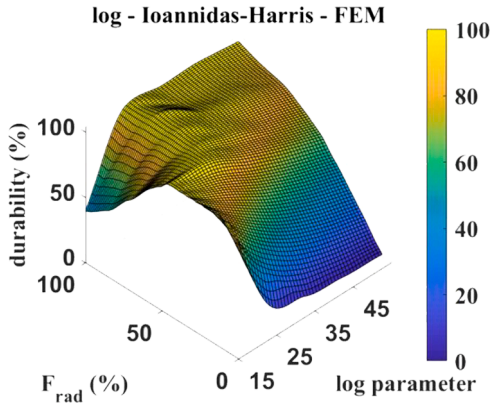

Fig. 33. 3D graph showing the ratio between the log parameter and the magnitude of the load on durability according to Ioannides-Harris.

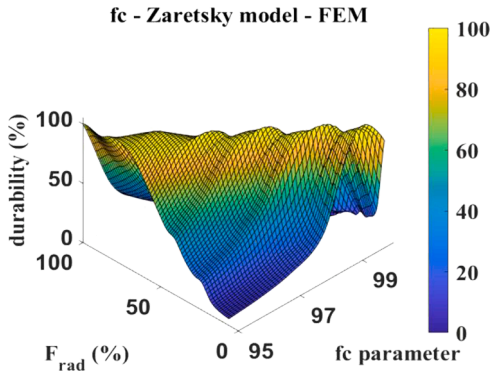

Fig. 34. 3D graph showing the ratio between the *fc* parameter and the magnitude of the load on durability according to Zaretsky.

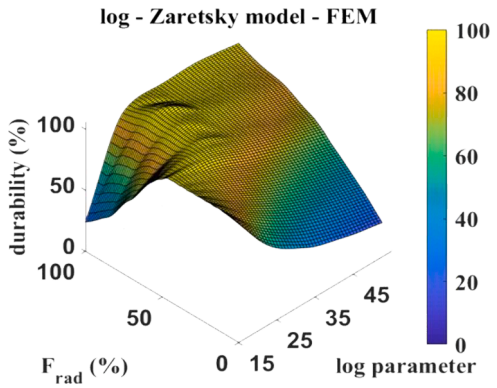

Fig. 35. 3D graph showing the ratio between the log parameter and the magnitude of the load on the durability according to Zaretsky.

5. Sensitivity analysis of the mesh grid element size

To prove the use of the right mesh grid density by all performed analyses, a mesh grid density sensitivity analysis was performed using various element size in the area of the rolling element radius, where the stress peaks were considered. This assumption was confirmed by former presented results.

The sensitivity analysis was done at the simplified detail of the model, which was also used by the analyses presented in the article. The model detail was analysed in the ¼ symmetry (Fig. 52).

The contact pair was observed. The type of mesh grid used was the same as by the former analyses presented in the article. The mesh grid density was changed only at the end radius of the small contact body by the values of 0.10, 0.20, **0.40**, 0.80 and 1.60 mm

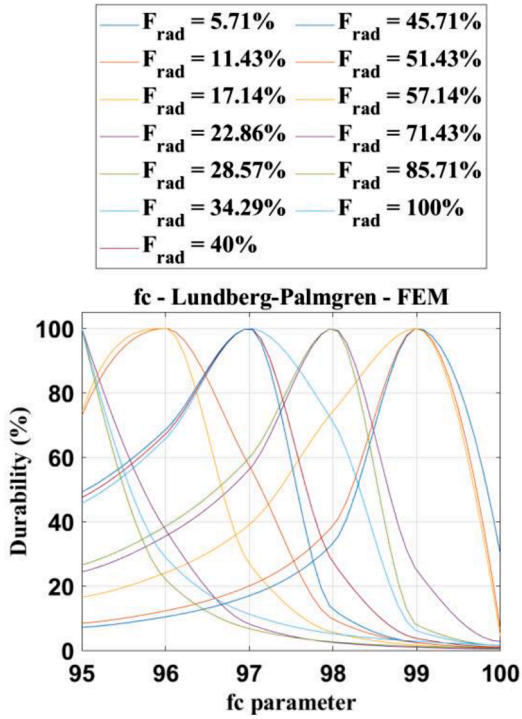

Fig. 36. Durability curves for selected bearing loads according to Lundberg-Palmgren for the *fc* profile.

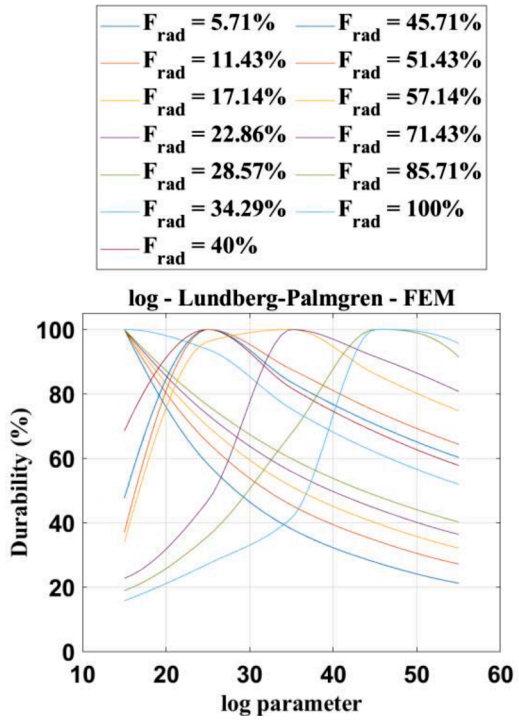

Fig. 37. Durability curves for selected bearing loads according to Lundberg-Palmgren for the log profile.

(Fig. 53), whereas the value of 0.40 mm was used by the analyses presented above.

The contact pressures were observed especially in the center of the rolling element and in the contact pressure peak location. The results of the sensitivity analysis by high load case are listed in Table 2, by medium load case in Table 3 and by low load case in Table 4.

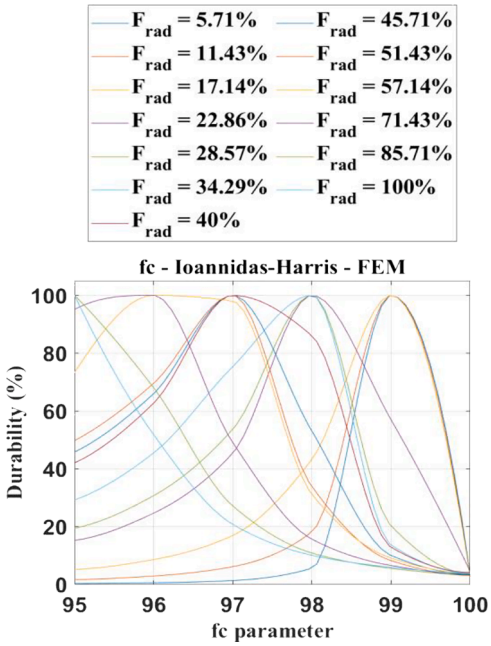

Fig. 38. Durability curves for selected bearing loads according to Ioannides-Harris for the *fc* profile.

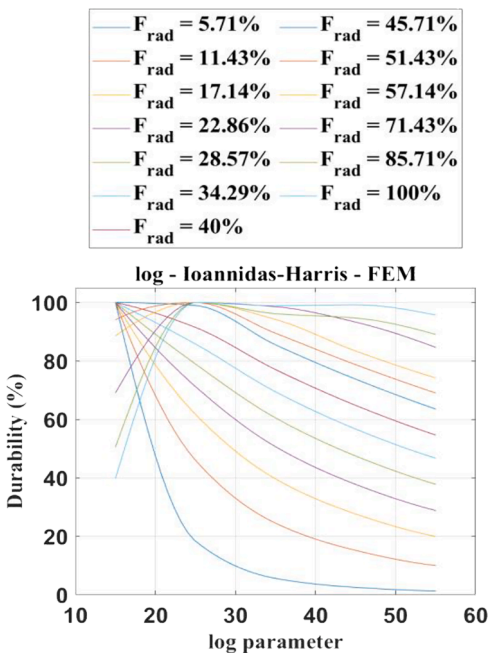

Fig. 39. Durability curves for selected bearing loads according to Ioannides-Harris for the log profile.

The adjacent radius mesh grid element size pressure difference Δ_M (%) in the presented tables are calculated by the equation

$$\Delta_M = \frac{|p_i - p_j|}{p_j}\ 100, \tag{21}$$

where: p_i – initial higher mesh grid element size (starting at 1.60 mm); p_j – following lower mesh grid element size (ending by 0.10 mm).

The various meshgrid element size contact pressure values by high load are presented in Fig. 54, by medium load in Fig. 55 and by

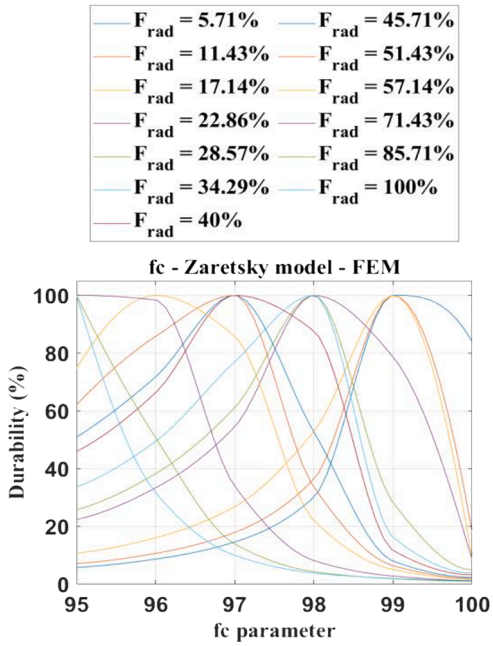

Fig. 40. Durability curves for selected bearing loads according to Zaretsky for the *fc* profile.

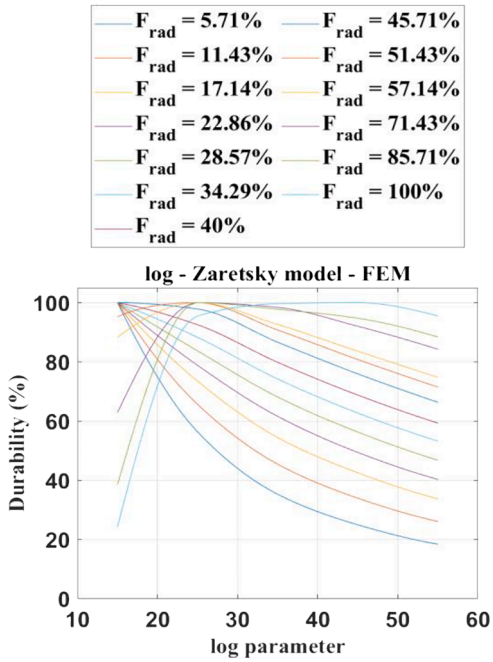

Fig. 41. Durability curves for selected bearing loads according to Zaretsky for the log profile.

low load in Fig. 56.

6. Discussion

The sensitivity analysis by the high load case showed, that if the end radius mesh grid changed from the 0.4 to 0.2 mm, the difference between the calculated contact pressure peaks was only 1.03%, which is a negligible difference (Table 2, Fig. 54). The small peak in Fig. 54 may be caused by a finite-element mesh error, but such a small value will not affect the results presented in this paper.

The sensitivity analysis by the medium load case showed, that if the end radius mesh grid changed from the 0.4 to 0.2 mm, the

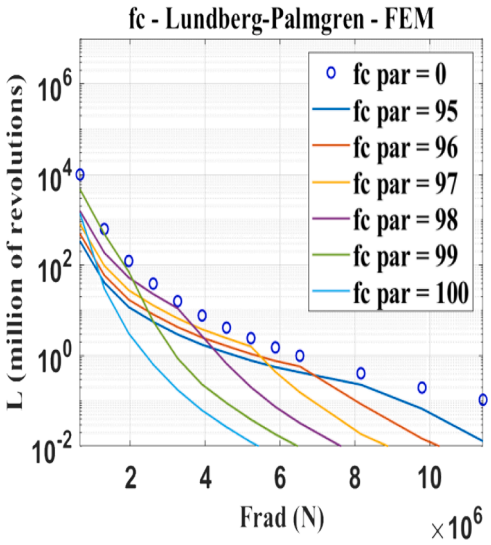

Fig. 42. Effect of the curves ratio size (*fc* parameter) on durability according to Lundberg-Palmgren at different load magnitudes.

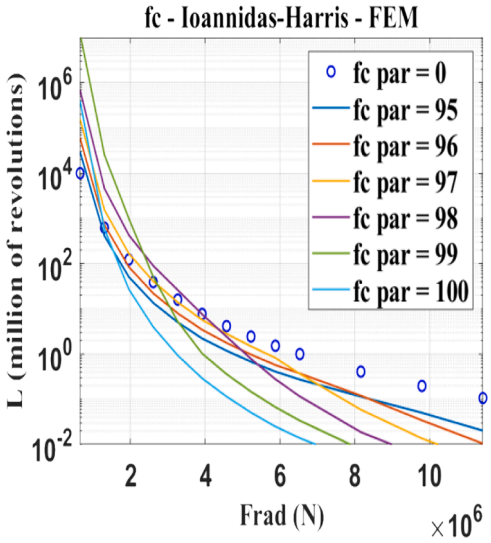

Fig. 43. Effect of the curves ratio size (*fc* parameter) on durability according to Ioannides-Harris at different load magnitudes.

difference between the calculated contact pressure peaks was only 0.23%, which is even less then by the high loads (Table 3, Fig. 55).

The sensitivity analysis by the low load case showed, that the end radius has not a significant impact on the stress peak, because of the contact pressure is distributed along the raceway without a peak. (Table 4, Fig. 56).

The chosen mesh grid element size of 0.4 mm is adequate to fulfill the goals, which should be achieved by the analyses presented in the article. Both finite element models were calculated with the same accuracy, thus the contact pressure values between the contact bodies of the models are calculated with the same accuracy too and the same relationship applies for the durability calculation. Based on these facts, we compare the relative durability difference between the standard *fc* profiled body and the log profile designed by us in the presented article.

The results of the FEM analyses presented in Figs. 6–11 are calculated using the FEM models with the chosen mesh grid element size supported by the sensitivity analysis. The more precise analysis of the load case presented in Figs. 6–10 (*fc* profile; low, medium and high load) is discussed below to prove that the finite element model error is low. At this stage we also performed analysis with various meshes. Stress peaks are observed in the direction of width of contact area at the ends of the contact length on both sides. The contact area is distributed in a narrow strip throughout the width (about $b = 2$ mm).

Fig. 57 to 59 show that the selected width of the contact surface is sufficient enough, because the contact pressure is not distributed over the entire inner and outer ring raceway and it has zero values at the edges as shown by the blue isosurface.

If the contact area reaches this part of the profile (which depends on the level of applied load), it is reasonable to find a stress peak.

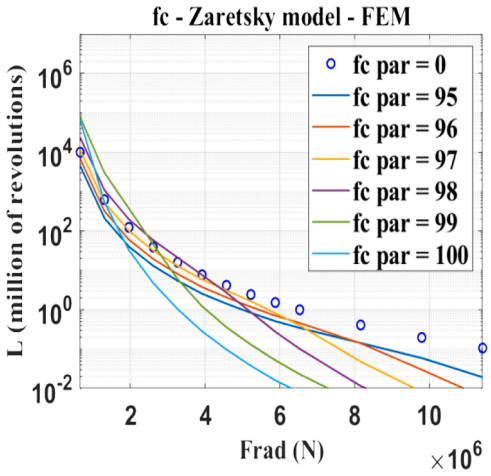

Fig. 44. Effect of the curves ratio size (*fc* parameter) on durability according to Zaretsky at different load magnitudes.

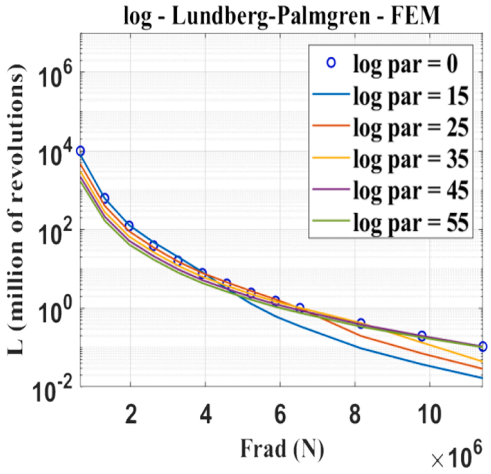

Fig. 45. Effect of the log parameter on durability according to Lundberg-Palmgren at different load magnitudes.

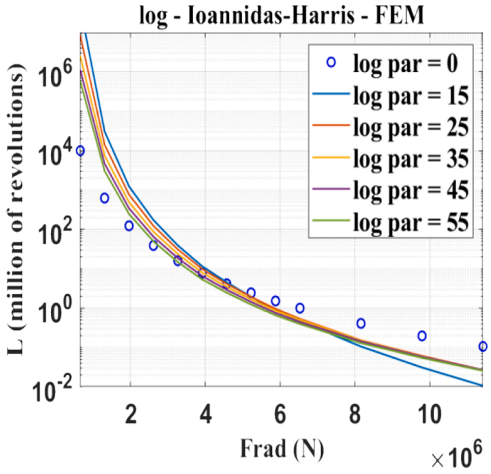

Fig. 46. Effect of the log parameter on durability according to Ioannides-Harris at different load magnitudes.

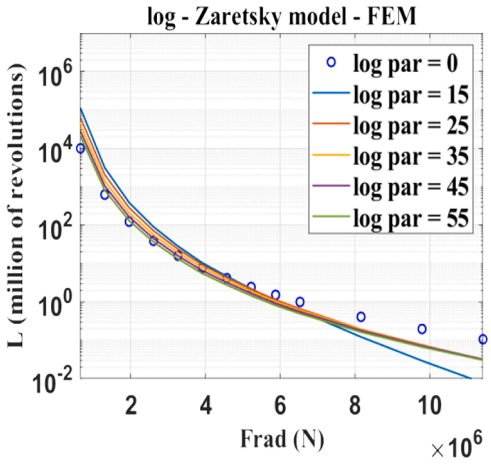

Fig. 47. Effect of the log parameter on durability according to Zaretsky in different load magnitudes.

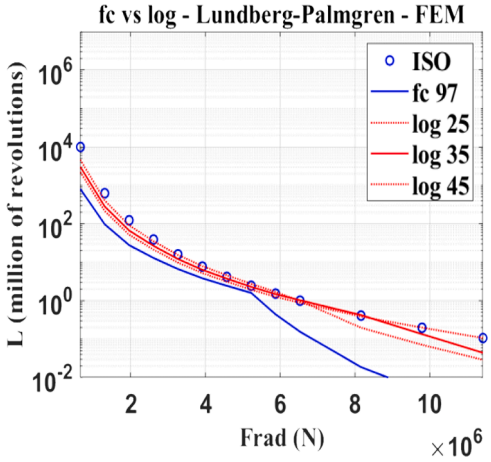

Fig. 48. Comparison of durability of selected values of the fc parameter and the log parameter according to Lundberg-Palmgren.

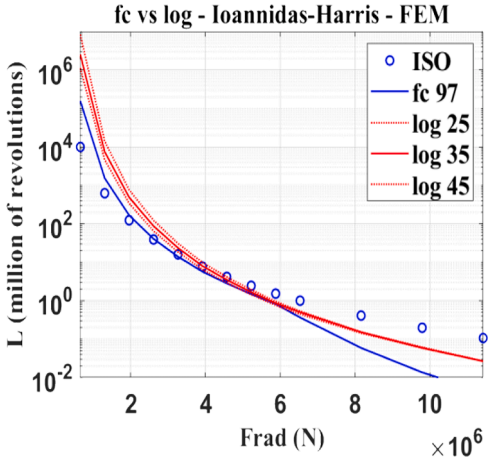

Fig. 49. Comparison of durability of selected values of the fc parameter and the log parameter according to Ioannides-Harris.

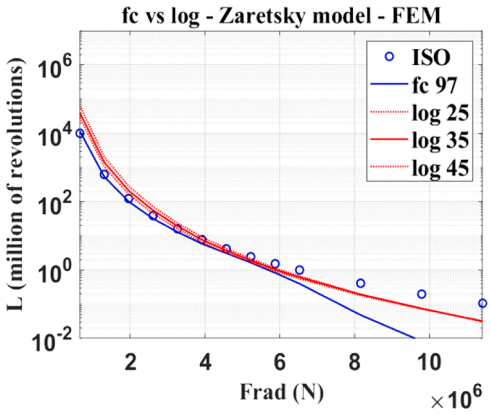

Fig. 50. Comparison of durability of selected values of the fc parameter and the log parameter according to Zaretsky.

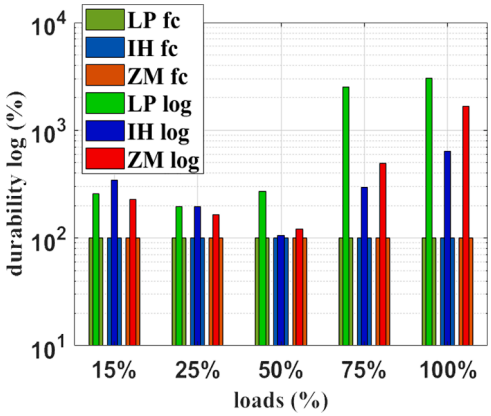

Fig. 51. Comparison of the increase in the durability of the shape of the element with the log profile calculated according to the selected theories at 100% durability of the shape of the rolling element with the fc profile for selected load magnitudes.

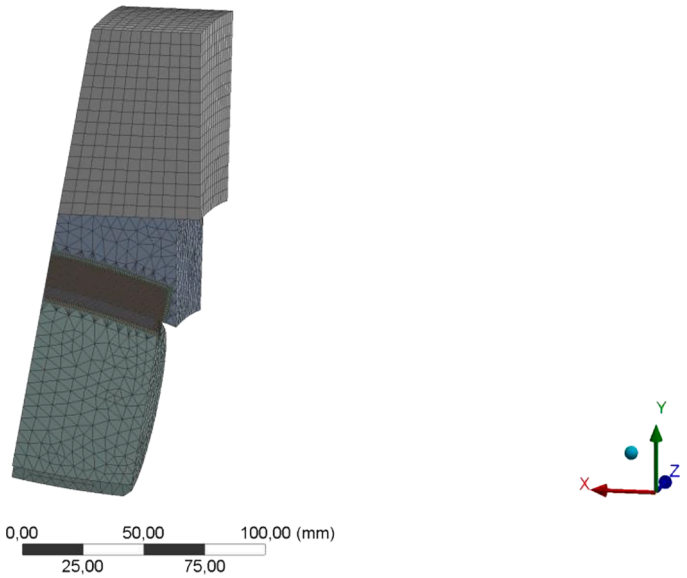

Fig. 52. Simplified contact detail model prepared for the sensitivity analysis.

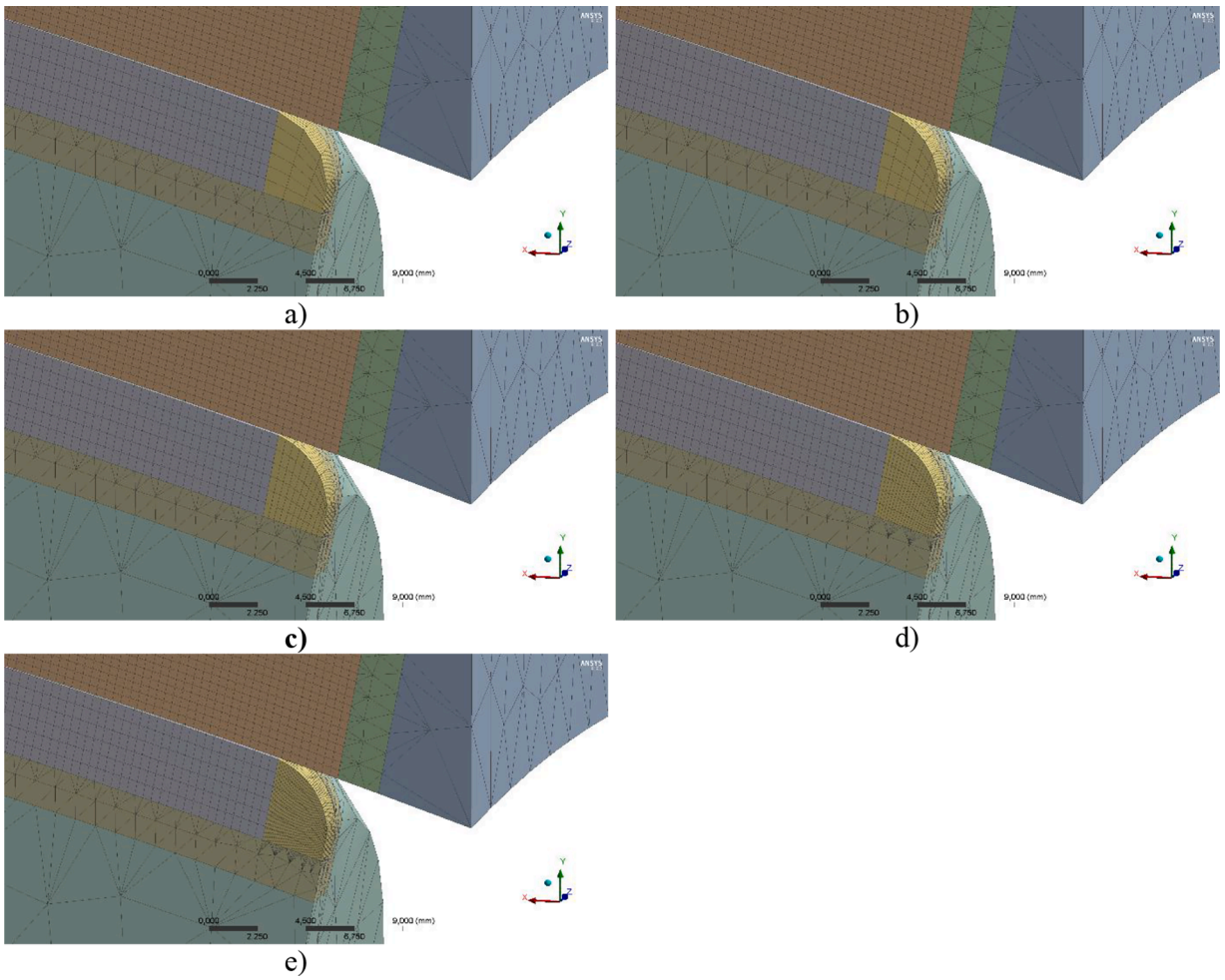

Fig. 53. Mesh grid density by various element dimension: (a) 1.60 mm; (b) 0.80 mm; **(c) 0.40 mm;** (d) 0.20 mm; (e) 0.10 mm.

Table 2
Mesh grid density sensitivity analysis by high load.

Radius element size (mm)		1.60	0.80	**0.40**	0.20	0.10
Contact pressure (MPa)	rolling element center	3194.40	3188.20	**3189.21**	3182.30	3182.40
	peak	5695.40	5428.40	**5306.40**	5361.30	5351.80
Adjacent peak pressure value difference (%)		–	4.69	**2.25**	1.03	0.18

Table 3
Mesh grid density sensitivity analysis by medium load.

Radius element size (mm)		1.60	0.80	**0.40**	0.20	0.10
Contact pressure (MPa)	rolling element center	1919.40	1919.30	**1919.20**	1919.00	1919.00
	peak	1375.50	1361.00	**1352.30**	1349.02	1349.00
Adjacent peak pressure value difference (%)		–	1.05	**0.64**	0.23	0.01

Figs. 60–62 show in detailed view of the end region of the Figs. 57–59 that the contact pressure peak is correctly distributed over the width of the contact area and it has the correct pressure gradient in all directions.

The results presented in Figs. 24–29 comparing the calculated durability for the individual models used by the appropriate theory are deeper discussed for the modified Fig. 27 presenting the results obtained by the Lundberg-Palmgren theory with marked goals of the analysis and calculations (Fig. 63).

The blue circles marked in the legend as ISO281 show the calculated dependence of durability on the load size according to the

Table 4
Mesh grid density sensitivity analysis by low load.

Radius element size (mm)		1.60	0.80	**0.40**	0.20	0.10
Contact pressure (MPa)	rolling element center	1157.00	1157.10	**1157.10**	1157.00	1157.00
	peak	–	–	**–**	–	–
Adjacent peak pressure value difference (%)		–	–	–	–	–

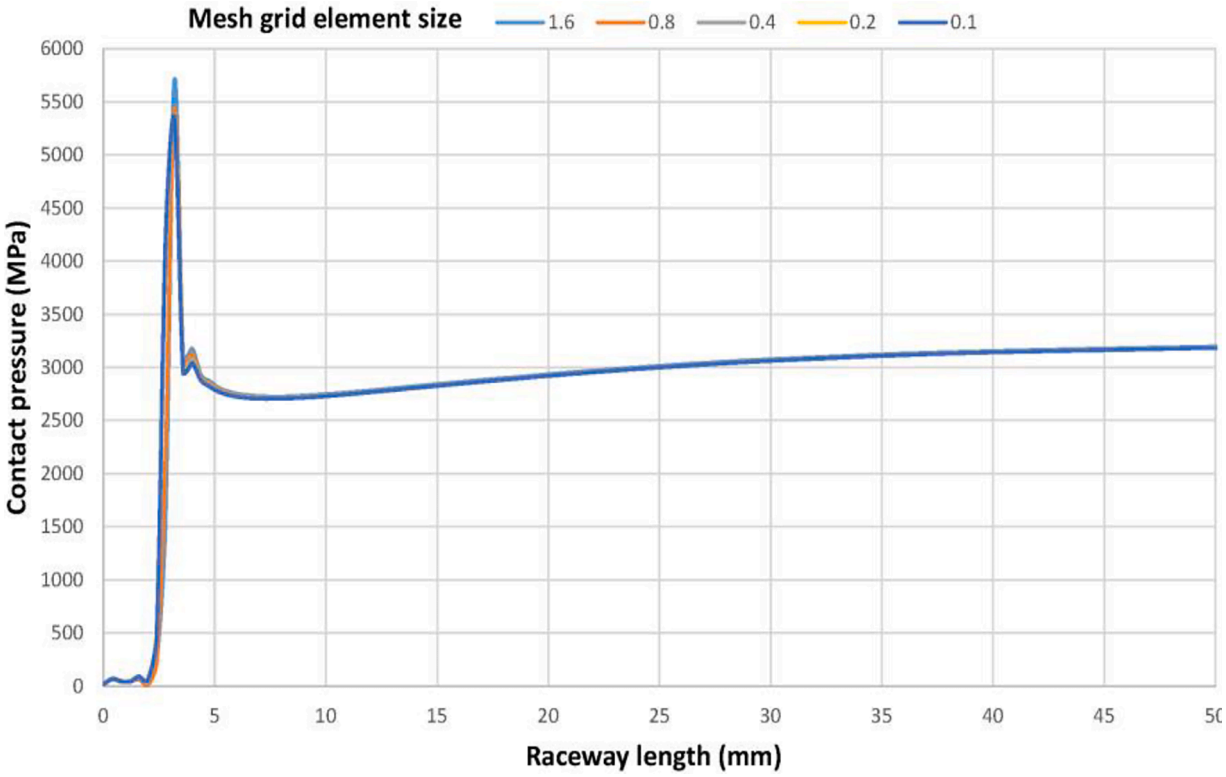

Fig. 54. Contact pressure along the raceway length by high load.

relevant theory by the ideal distribution of contact pressure without a pressure peak (with the same size along the entire length of the line contact). However, we have calculated a real profile of contact bodies, in which the distribution of contact pressure is not ideal. The calculations and results in the article have shown that the contact pressure peaks occur at the ends of the body profile at large load values. These pressure peaks affect the calculated durability according to the individual theories.

Fig. 63 shows, that the contact pressure peak of the standard barrel bearing *fc* profile (blue square) appears already at lower loads and its calculated durability is lower than by the ideal pressure distribution according ISO281 (left offset from the ISO 281 curve). The proposed *log* profile succeeded to achieve a more favorable distribution of contact pressure with smaller pressure peaks at higher loads than the standard *fc* profile (red square). The calculated *log* profile curve shows that its durability is higher for the same load as applied by the *fc* profile and the pressure contact peak affects the durability first at higher load values than in the case of the *fc* profile even by smaller durability drop gradient (area above the red square).

7. Conclusion

This paper deals with the increase of the durability in the area of the line contact with curved bodies. The presented results show that surprisingly at medium magnitudes by approximately 50% of maximum possible load of the line contact (curved – spherical roller / toroidal) the benefit of the logarithmic profile is minimal – the calculated durability has almost been identical to the initial state. However, at low load magnitudes (15–25% of max. load), the durability calculated for the logarithmic profile has approximately

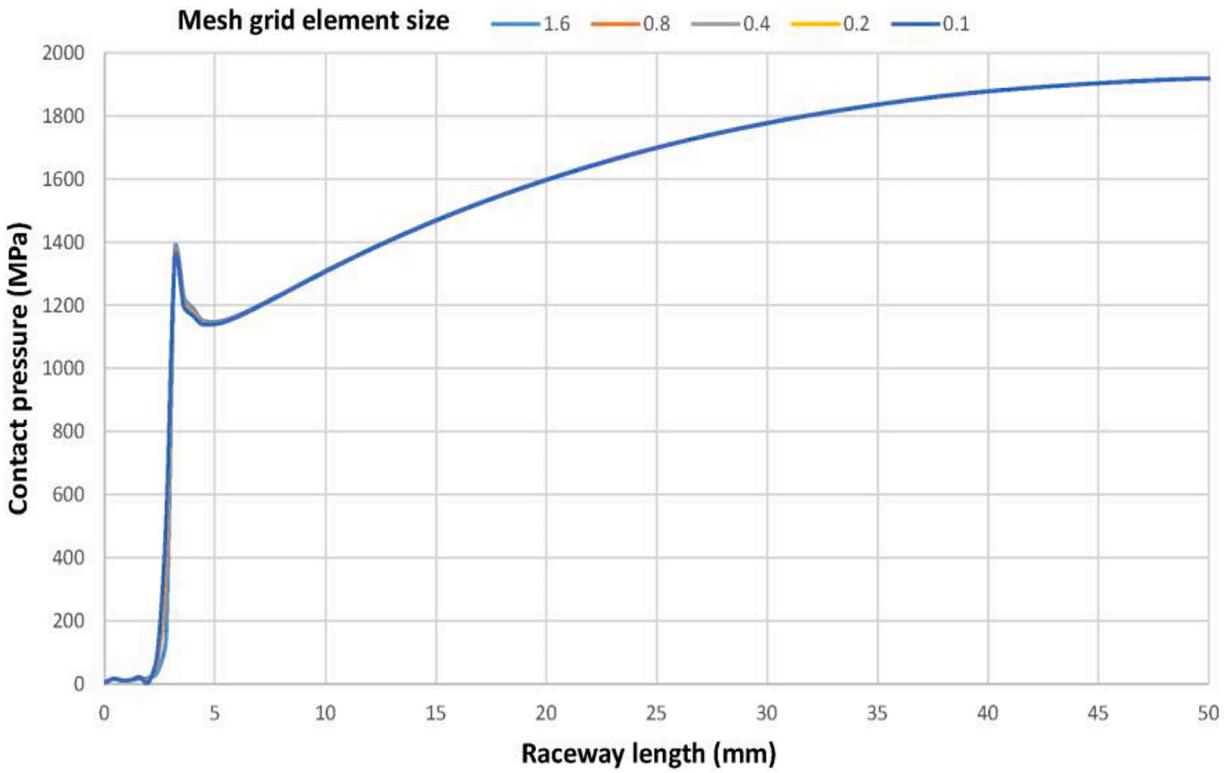

Fig. 55. Contact pressure along the raceway length by medium load.

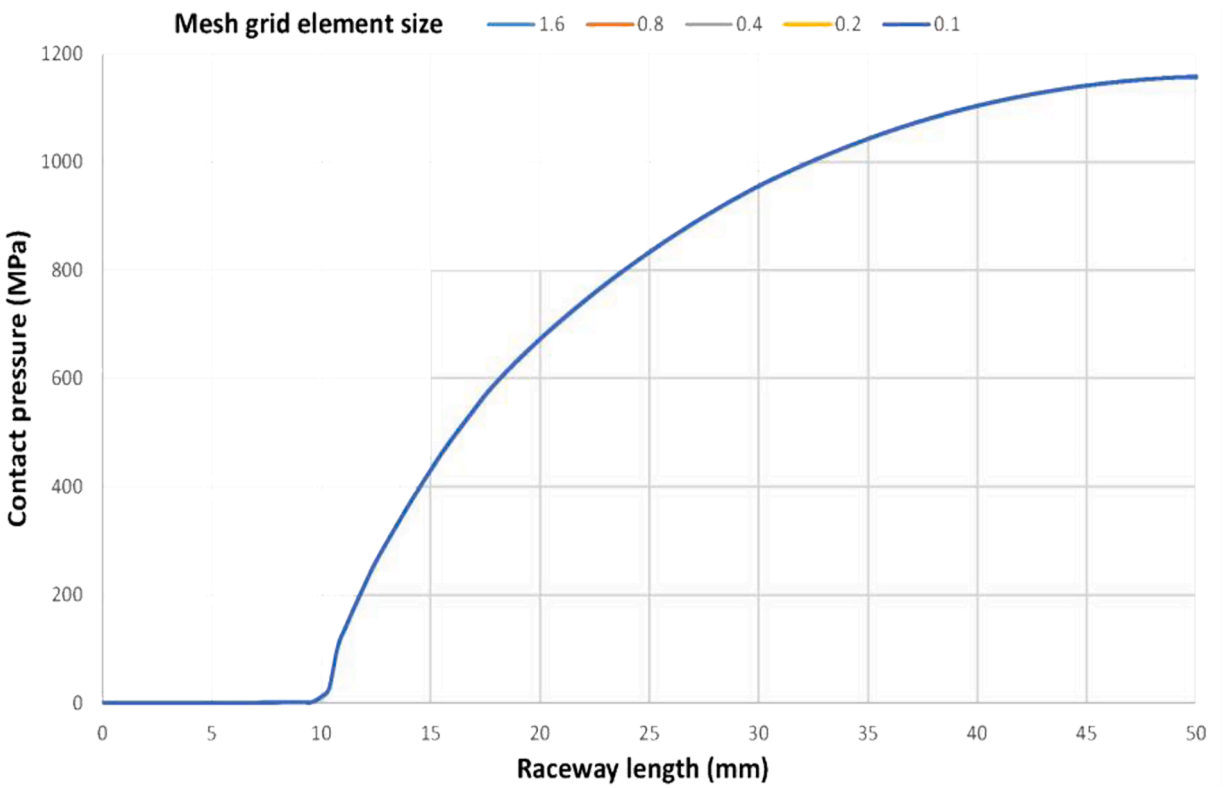

Fig. 56. Contact pressure along the raceway length by low load.

doubled. For example, if a spherical roller bearing with a fully crowned (*fc* profile) profile reaches 1,000,000 revolutions, then the same bearing with a logarithmic shape of the rolling element (*log* profile) should last approximately 2,000,000 revolutions at identical load. At high load magnitudes (80–100% of max. load), the calculated durability has multiplied several times, which is caused due to the fact that the logarithmic profile successfully eliminates stress peaks at the end profiles.

The benefit of the solution is very desirable from the point of view of the increase in the durability of machine parts. Of course, there should be mentioned that the production costs will increase, since it is easier to grind, e.g., the bearing's rolling element profiles with the common *fc* profile than to manufacture a new shape tool with a specific *log* profile. However, not all applications are expected to be produced using this logarithmic profile – this application is suitable for special applications such as large wind turbine bearings etc., where there are high stresses caused by the loading and every percentage increase in theoretical durability is of great importance. Furthermore, the use of the logarithmic profile reduces the contact and subsurface stresses, eliminates stress peaks and thus makes it possible to reduce the dimensions of the bearing rings. Each of these eliminations has a significant benefit in reducing weight, as the weight of, e.g., large bearing equals hundreds of kilograms. Material cost savings are also directly related to the weight saving, because high-quality materials are used to produce such large mechanical parts.

Nomenclature

Symbol	Meaning	Unit
A	- material constant	[-]
b_m	- coefficient of basic dynamic load rating	[-]
b	- contact volume width	[mm]
C_r	- basic dynamic load rating	[kN]
c	- represents the exponent of the critical shear stress	[-]
D_E	- diameter of the raceway of the outer ring	[mm]
D_F	- diameter of the raceway of the inner ring	[mm]
D_{we}	- rolling element diameter	[mm]
d_{log}	- logarithmic parameter	[-]
E	- Young's modulus	[MPa]
E_O	- planar stress	[MPa]
$E_{I,II}$	- Young's modulus of the respective bodies	[-]
e	- Weibull slope	[-]
f_c	- coefficient depending on bearing geometry and accuracy of production and material	[-]
h	- material constant	[-]
i	- number of rows of rolling elements	[-]
L_{10}	- basic rating life	[10^6 revs]
l_{ef}	- effective length of rolling element	[mm]
l_T	- maximum length of rolling element	[mm]
N	- reload cycles	[-]
P_e	- equivalent dynamic bearing load	[kN]
p	- exponent, bearing determination constant	[-]
p_i	- initial higher mesh grid element size	[mm]
p_j	- following lower mesh grid element size	[mm]
p_0	- contact stress	[MPa]
Q	- acting load at the point of contact	[N]
Q_{max}	- maximum load of rolling element	[N]
q	- curvature of raceways and rolling elements	[mm^{-1}]
R_e	- radius of the raceway of the outer ring	[mm]
S	- probability of survival	[-]
V	- stressed volume	[mm^3]
Z	- number of rolling elements	[-]
z_0	- depth of applied shear stress	[mm]
$2b$	- minor axis of the ellipse in contact	[mm]
α	- contact angle	[°]
μ	- Poisson's constant	[-]
Δ	- adjacent contact pressure difference	[-]
Δ_M	- pressure difference of adjacent grid elements	[-]
π	- Ludolf's constant	[-]
τ	- critical shear stress	[MPa]
τ_0	- shear stress	[MPa]
τ_u	- limit fatigue stress	[mpa]

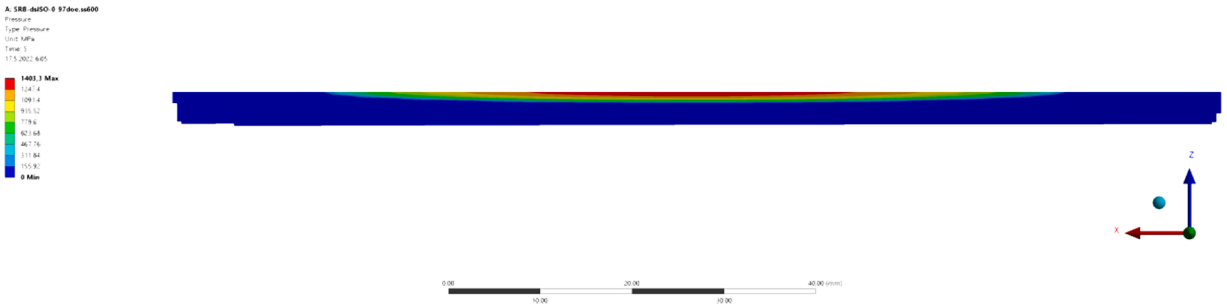

Fig. 57. Detailed view on the contact pressure values at the inner ring raceway by low load in half symmetry (For interpretation of the references to color in this figure legend, the reader is referred to the web version of this article.).

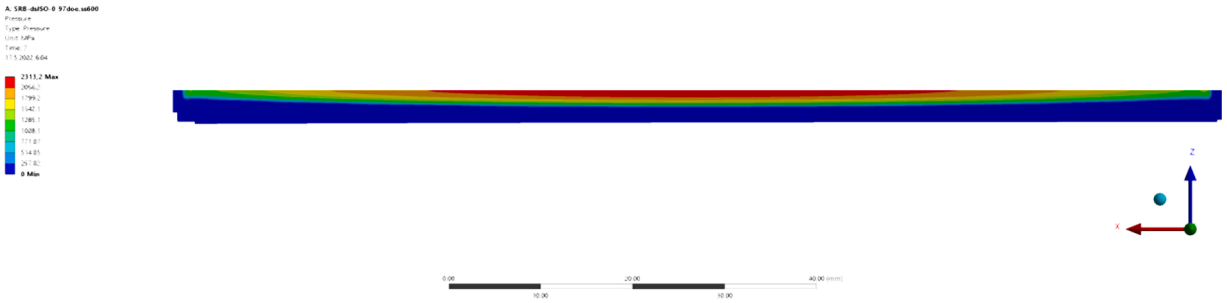

Fig. 58. Half view on the contact pressure values of the inner ring raceway by medium load (For interpretation of the references to color in this figure legend, the reader is referred to the web version of this article.).

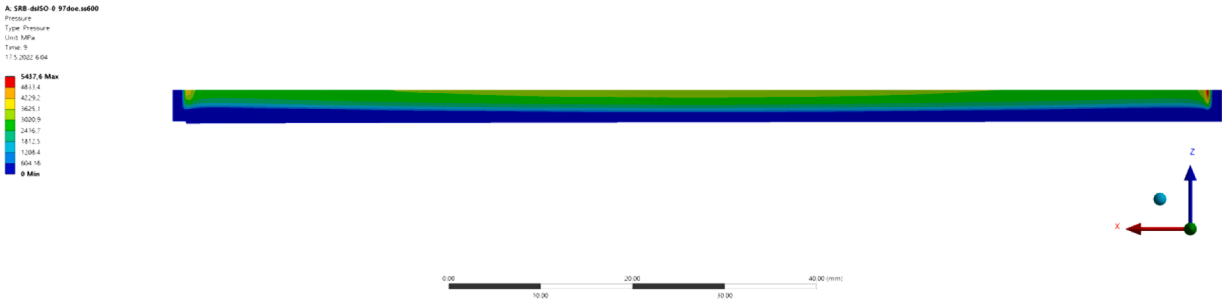

Fig. 59. Half view on the contact pressure values of the inner ring raceway by high load (For interpretation of the references to color in this figure legend, the reader is referred to the web version of this article.).

Declaration of Competing Interest

The authors declare that they have no known competing financial interests or personal relationships that could have appeared to influence the work reported in this paper.

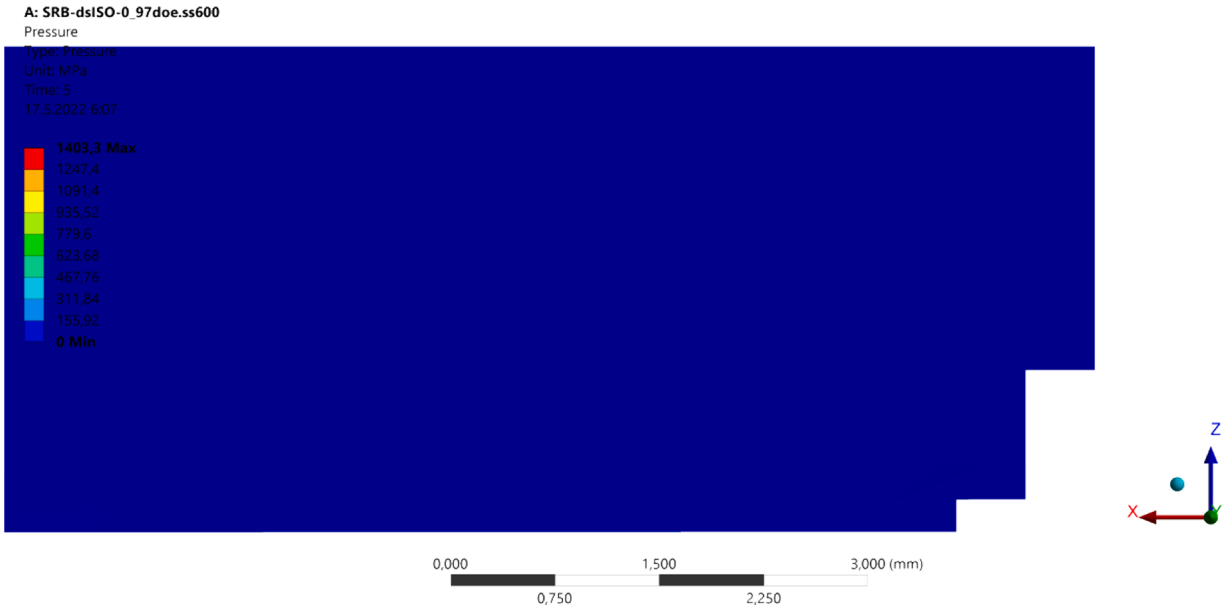

Fig. 60. Detailed view of the Fig. 57 showing the contact pressure peaks at the inner ring raceway end by low load.

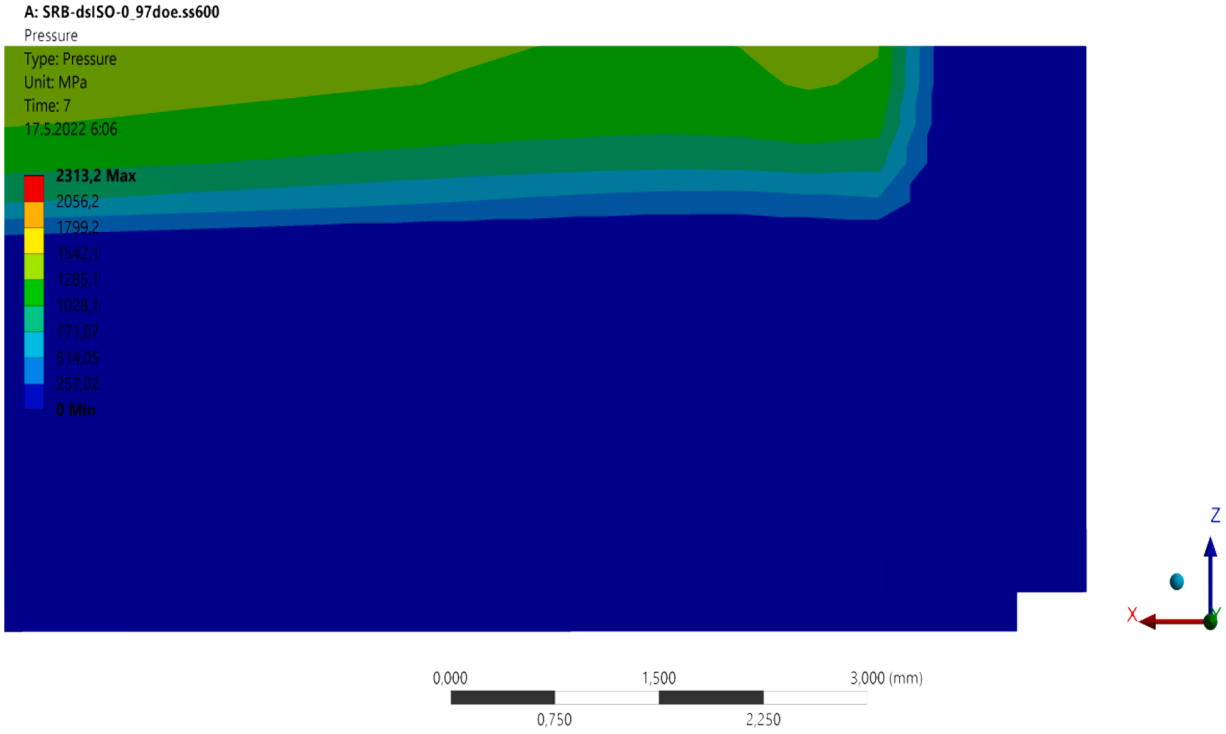

Fig. 61. Detailed view of the Fig. 58 showing the contact pressure peaks at the inner ring raceway end by medium load.

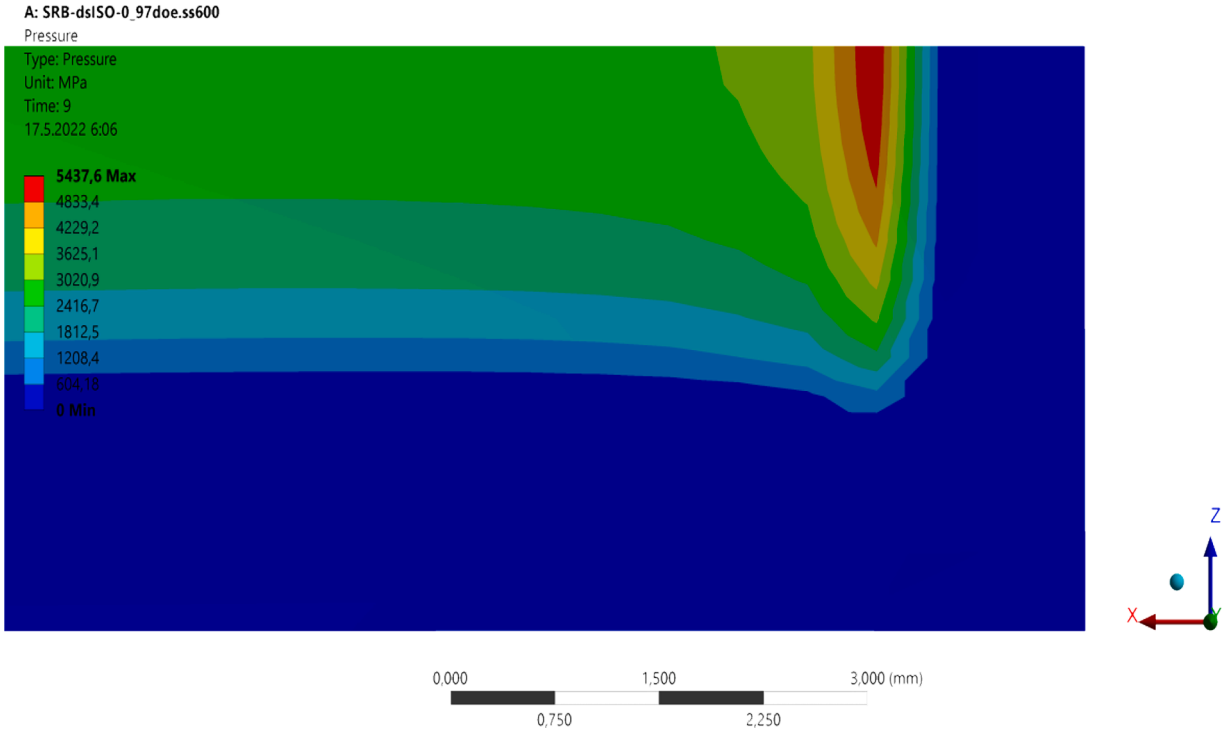

Fig. 62. Detailed view of the Fig. 59 showing the contact pressure peaks at the inner ring raceway end by high load.

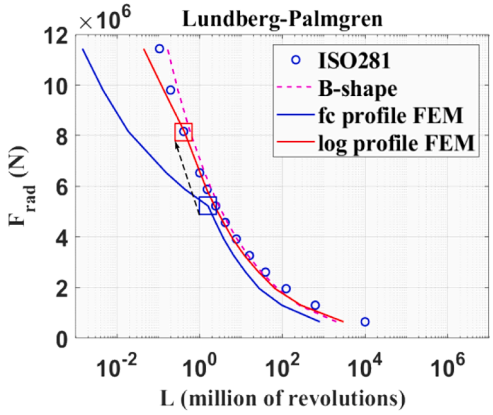

Fig. 63. Difference between various profiles durability calculations according to Lundberg-Palmgren theory (For interpretation of the references to color in this figure legend, the reader is referred to the web version of this article.).

Acknowledgment

This study was supported by Ministry of Education, Science, Research and Sport under the contract No. 1/0595/18 – optimising the internal geometry of roller bearings with line contact in order to increase their durability and reduce their structural weight.

References

[1] Z. Yanfei, F. Bin, K. Lingfei, L. Yan, Effect of the ring misalignment on the service characteristics of ball bearing and rotor system, Mech. Mach. Theory 151 (2020), 103889. UNSP.
[2] G. Chen, G. Wen, Z. Xiao, H San, Experimental study on contact force in a slewing bearing, ASME. J. Tribol. 140 (2) (2018), 021402.
[3] I. Heras, J. Aguirrebeitia, M. Abasolo, I. Coria, An engineering approach for the estimation of slewing bearing stiffness in wind turbine generators, Wind Energy 22 (2018) 376–391.
[4] A. Golubenko, A. Kostyukevich, I. Tsyganovskiy, V. Nozhenko, The influence of a rail lateral bending on the stress – strain state of a wheel - rail contact, Teka Comm. Mot. Power Ind. Agric. 11a (2011) 78–84.

[5] Y. Han, L. Yang, T. Xu, Analysis of static stiffness fluctuation in radially loaded ball and roller bearings, Arch. Appl. Mech. 91 (4) (2021) 1–16, https://doi.org/10.1007/s00419-020-01853-6.
[6] International Organization for Standardization, ISO 281:2007(en): Rolling bearing - dynamic load ratings and rating life, 2007.
[7] G. Lundberg, A. Palmgren, Dynamic capacity of rolling bearings, in: Acta Polytechnica, Mechanical Engineering Series 2, 3, Royal Swedish Academy of Engineering Sciences, 1947, p. 7.
[8] J. Kaczor, A. Raczyński, The influence of preload on the work of angular contact ball bearings, Arch. Mech. Eng. 63 (3) (2016) 319–336.
[9] E. Ioannides, T. Harris, A new fatigue life model for rolling bearings, ASME J. Tribol. 107 (1985) 367–378.
[10] W. Weibull, A Statistical Theory of the Strength of Materials, Royal Swedish Academy of Engineering Sciences Proceeding, 1939, p. 151.
[11] E.V. Zaretsky, Rolling bearing life prediction, theory and application. Recent Developments in Wear Prevention, Friction and Lubrication, Research Signpost, Kerala, India, 2010, pp. 45–136. ISBN: 978-81-308-0377-7.
[12] E.V. Zaretsky, Design for life, plan for death, Mach. Des. 66 (15) (1994) 55–59.
[13] E. Askari, Mathematical models for characterizing non-Hertzian contacts, Appl. Math. Model. 90 (2021) 432–447, https://doi.org/10.1016/j.apm.2020.08.048.
[14] M.J. Lewandowski-Szewczyk, S. Stupkiewicz, Non-standard contact conditions in generalized continua: microblock contact model for a Cosserat body, Int. J. Solids Struct. 202 (2020) 881–894, https://doi.org/10.1016/j.ijsolstr.2020.07.001.
[15] F. Brumercik, M. Lukac, J. Caban, Z. Krzysiak, A. Glowacz, Comparison of selected parameters of a planetary gearbox with involute and convex-concave teeth flank profiles, Appl. Sci. Basel 10 (4) (2020) 1417, https://doi.org/10.3390/app10041417.
[16] P. Weis, L. Kucera, P. Pechac, M. Mocilan, Modal analysis of gearbox housing with applied load, Procedia Eng. 192 (2017) 953–958, https://doi.org/10.1016/j.proeng.2017.06.164.
[17] S. Gramblicka, R. Kohar, M. Majchrak, M. Vrabec, Contact analysis of selected toothed contact of the two-stage front gearbox, Curr. Methods Constr. Des. Lect. Notes Mech. Eng. 1 (2020) 263–269.
[18] H. Ghaednia, R. Jackson, H. Lee, A. Rostami, X Wang, Contact mechanics, in: P.L. Menezes, M. Nosonovsky, S.P. Ingole, S.V. Kailas, M.R. Lovell (Eds.), Tribology for Scientists and Engineers, Springer Science+Business Media, New York, 2013, pp. 93–140, https://doi.org/10.1007/978-1-4614-1945-7_3.
[19] M. Drbul, P. Martikan, J. Broncek, I. Litvaj, J. Svobodova, Analysis of roughness profile on curved surfaces, Innov. Technol. Eng. Prod. 244 (2018) 01024, https://doi.org/10.1051/matecconf/201824401024 (ITEP'18).
[20] M.R. Hoeprich, H. Zantopulos, Line contact deformation – a cylinder between 2 flat plates, J. Lubr. Technol.Trans. ASME 103 (1) (1981) 21–25.
[21] A. Xiaolan, C.H. Moyer, Rolling Element Bearings, CRC Press LLT, Ohio, 2001, p. 53.
[22] Z. Wu, Y. Xu, K. Liu, Study on logarithmic crowning of tapered roller profile considering angular misalignment, ASME. J. Tribol. 142 (11) (2020), 111201, https://doi.org/10.1115/1.4047106.
[23] Z. Wu, Y. Xu, S. Deng, et al., Study on logarithmic crowning of cylindrical roller profile considering angular misalignment, J. Mech. Sci. Technol. 34 (2020) 2111–2120, https://doi.org/10.1007/s12206-020-0130-7.
[24] P. He, Y. Wang, H. Liu, et al., Optimization design of structural parameters of single-row four-point contact ball slewing bearing, J. Braz. Soc. Mech. Sci. Eng. 42 (2020) 291, https://doi.org/10.1007/s40430-020-02391-6.
[25] M. Majchrak, R. Kohar, M. Lukac, R. Skyba, The process of creating a computational 3D model of a harmonic transmission, MM Sci.J. (2020) 3926–3931, https://doi.org/10.17973/MMSJ.2020_06_2020009.
[26] M. Majchrak, R. Kohar, J. Kajan, R. Skyba, 3D meshing methods of ball-rolling bearings, Transp. Res. Procedia 40 (2019) 784–791, https://doi.org/10.1016/j.trpro.2019.07.111.
[27] R. Skrypnyk, J.C.O. Nielsen, M. Ekh, et al., Metamodelling of wheel–rail normal contact in railway crossings with elasto-plastic material behaviour, Eng. Comput. 35 (2019) 139–155, https://doi.org/10.1007/s00366-018-0589-3.
[28] Q. Wen, Q. Du, X. Zhai, An analytical method for calculating the tooth surface contact stress of spur gears with tip relief, Int. J. Mech. Sci. 151 (2019) 170–180, https://doi.org/10.1016/j.ijmecsci.2018.11.007.